Critical Review of UV-Advanced Reduction Processes for the Treatment of Chemical Contaminants in Water

Benjamin D. Fennell, Stephen P. Mezyk, and Garrett McKay*

Cite This: *ACS Environ. Au* 2022, 2, 178−205

Read Online

ACCESS | Metrics & More | Article Recommendations | Supporting Information

ABSTRACT: UV-advanced reduction processes (UV-ARP) are an advanced water treatment technology characterized by the reductive transformation of chemical contaminants. Contaminant abatement in UV-ARP is most often accomplished through reaction with hydrated electrons (e_{aq}^-) produced from UV photolysis of chemical sensitizers (e.g., sulfite). In this Review, we evaluate the photochemical kinetics, substrate scope, and optimization of UV-ARP. We find that quantities typically reported in photochemical studies of natural and engineered systems are under-reported in the UV-ARP literature, especially the formation rates, scavenging capacities, and concentrations of key reactive species like e_{aq}^-. The absence of these quantities has made it difficult to fully evaluate the impact of operating conditions and the role of water matrix components on the efficiencies of UV-ARP. The UV-ARP substrate scope is weighted heavily toward contaminant classes that are resistant to degradation by advanced oxidation processes, like oxyanions and per- and polyfluoroalkyl substances. Some studies have sought to optimize the UV-ARP treatment of these contaminants; however, a thorough evaluation of the impact of water matrix components like dissolved organic matter on these optimization strategies is needed. Overall, the data compilation, analysis, and research recommendations provided in this Review will assist the UV-ARP research community in future efforts toward optimizing UV-ARP systems, modeling the e_{aq}^--based chemical transformation kinetics, and developing new UV-ARP systems.
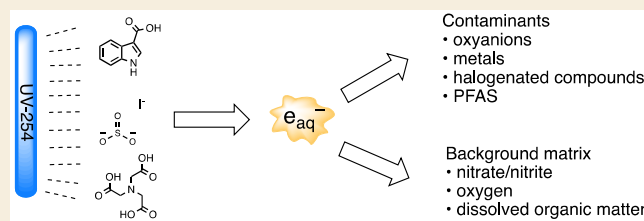
KEYWORDS: photochemistry, UV-ARP, water treatment, hydrated electron, PFOA, PFOS, PFAS, reduction, water quality, contaminants

1. INTRODUCTION

Ultraviolet-based advanced reduction processes (UV-ARP) have received significant attention in recent years for the treatment of several classes of recalcitrant chemical contaminants in water.[1−7] Advanced reduction processes are based on production of highly reducing hydrated electrons (e_{aq}^-, Figure 1),
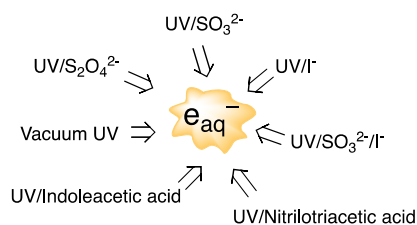
Figure 1. Summary of UV-advanced reduction processes (UV-ARP) generation of hydrated electrons (e_{aq}^-).

which exhibit fast bimolecular reaction rate constants with inorganic and organic compounds.[8] In UV-ARP, e_{aq}^- are produced by the illumination of e_{aq}^- sensitizers with UV lamps. Photoproduced e_{aq}^- can react with target contaminants (TC), leading to TC transformation. Given its high reactivity, e_{aq}^- is also scavenged by various chemical species naturally present in water.

The need for UV-ARP is motivated by the fact that many pollutants commonly found in contaminated waters are not readily treated by UV-advanced oxidation processes (UV-AOP), one of the most widely used degradative technologies in advanced water treatment. The need for an alternative to in situ oxidation processes has been recognized for some time. A patent by Bolton and Cater in 1993 detailing the treatment of wastewater or groundwater containing chloroform as a model halogenated organic with UV/iodide, UV/thiosulfate, UV/sulfite, and UV/iodide/thiosulfate as the e_{aq}^- source was one of the first reports of this technology.[9] Subsequent UV-ARP studies have focused on substrates that can undergo reduction by e_{aq}^- reaction such as oxyanions,[6,10−19] highly oxidized elements (e.g., Cr(VI)),[20,21] halogenated disinfection byproducts,[5,6,16] and per- and polyfluoroalkyl substances (PFAS).[22−34] Several bench-scale studies[22−31] and a recent pilot-scale[32] demonstration suggest that UV-ARP is one of the more promising technologies

for degrading PFAS, which are resistant to direct photolysis and UV-AOP.[22,23,35]

Despite the promise of UV-ARP, implementation of these technologies at the large scale has not been realized. Given the high level of research activity of UV-ARP for the e_{aq}^--based transformation of contaminants over the past decade, there is a critical need to understand the limitation of these technologies from both chemical and engineering perspectives. While recent publications have reviewed various aspects of UV-ARP, like specific e_{aq}^- sensitizer systems (e.g., UV-sulfite[3,36,37]) or applicability toward certain contaminant classes (e.g., PFAS[2,38]), a comprehensive review of UV-ARP technologies is lacking. The objective of this Review is therefore to critically evaluate the factors influencing the effectiveness of UV-ARP for the degradation of contaminants in water. We summarize and review the UV-ARP literature for treatment of some important inorganic and organic contaminants, identify the knowledge gaps and potential limitations for these technologies, and suggest paths forward for research in this field. This is accomplished by presenting the photochemical kinetics of e_{aq}^- production and scavenging in UV-ARP, reviewing the sensitizers that have been employed to generate e_{aq}^- in UV-ARP, examining the classes of contaminants for which UV-ARP treatment has been studied, and highlighting novel UV-ARP technologies that seek to increase the rate of target contaminant degradation. The data compilation and perspectives provided in this review will assist the UV-ARP research community in future efforts to optimize UV-ARP systems, model the e_{aq}^--based transformation kinetics, and develop novel UV-ARP systems.

2. PRODUCTION AND SCAVENGING OF HYDRATED ELECTRONS IN UV-ARP

In UV-ARP, target contaminants are degraded through direct photolysis or through reaction with photochemically generated e_{aq}^{-}[9,39] (Figure 2). Considering the latter, indirect, photolysis

$$TC \xrightarrow{h\nu} product \quad \textit{direct photolysis}$$

indirect photolysis

$$sens^n \xrightarrow{h\nu} sens^{n+1} + e_{aq}^-$$
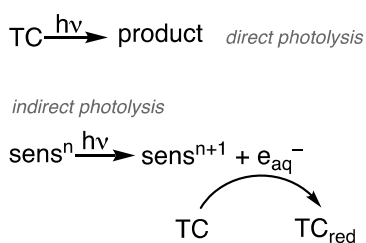$$TC \qquad TC_{red}$$

Figure 2. Direct and indirect (i.e., sensitized) photochemical transformation of a target contaminant in UV-ARP. The sensitizer charge (n) increases by +1 upon photoionization.

pathway, the rate of target contaminant transformation in UV-ARP systems is a function of both the intrinsic reactivity of the contaminant with e_{aq}^- (its bimolecular reaction rate constant) and the concentration of e_{aq}^-. The bimolecular rate constant for a target contaminant with e_{aq}^- is a constant value under specific solution conditions (e.g., temperature, ionic strength). Thus, strategies to optimize UV-ARP must aim to increase the exposure of the contaminant to e_{aq}^-, by increasing either the irradiation time or the hydrated electron concentration, $[e_{aq}^-]$. Increasing $[e_{aq}^-]$ can be accomplished through multiple means, such as using higher wattage lamps, increasing sensitizer concentrations, and minimizing the rate of interfering e_{aq}^- scavenging reactions. Understanding the factors that influence $[e_{aq}^-]$ is therefore an important consideration in UV-ARP studies.

The sections below address these factors by using established photochemical kinetic models to describe the rate of e_{aq}^--based contaminant transformation, the chemistry of known e_{aq}^- sensitizers, and the scavenging kinetics of e_{aq}^- in water. We end this section by focusing on knowledge gaps in this area, primarily the lack of a standardized measurement protocol for quantifying $[e_{aq}^-]$ in UV-ARP.

2.1. Transformation of a Target Contaminant by Hydrated Electrons

The rate law for the loss of a target contaminant (TC) in UV-ARP, which can be due both to direct photolysis and e_{aq}^--sensitized reactions, is given by

$$\frac{d[TC]}{dt} = -(k_d' + k_{TC,e_{aq}^-}[e_{aq}^-])[TC] \tag{2.1}$$

where k_d' is the pseudo-first-order rate constant of TC by direct photolysis (s^{-1}), k_{TC,e_{aq}^-} is the TC-e_{aq}^- bimolecular reaction rate constant $(M^{-1}\ s^{-1})$, $[TC]$ is the concentration (M) of TC remaining, and $[e_{aq}^-]$ is the concentration (M) of hydrated electron.[40] Equation 2.1 can be simplified by assuming that $[e_{aq}^-]$ remains at a steady-state throughout the treatment process, resulting in the expression

$$\frac{d[TC]}{dt} = -(k_d' + k_{TC}')[TC] \tag{2.2}$$

where k_{TC}' is a first-order rate constant $(k_{TC}' = k_{TC,e_{aq}^-}[e_{aq}^-]_{ss})$. Equations 2.1 and 2.2 forms the basis of all photochemical kinetic models for describing the time dependence of $[TC]$. Equation 2.1 can be further specified by including equations that describe the formation and scavenging of e_{aq}^-. For example, if $[e_{aq}^-]$ cannot be approximated as steady-state, then the time-dependent $[e_{aq}^-]$ can be described by

$$[e_{aq}^-]_t = \frac{R_{f,t}^{e_{aq}^-}}{k_{S,t}'} \tag{2.3}$$

where $R_{f,t}^{e_{aq}^-}$ represents the formation rate of e_{aq}^- $(M\ s^{-1})$ and $k_{S,t}'$ represents the total e_{aq}^- scavenging capacity, all as a function of time t.

In UV-ARP, e_{aq}^- is typically formed by illumination of a chemical sensitizer by UV lamps. Under monochromatic conditions (e.g., a low-pressure Hg lamp), eq 2.3 can be expanded to eq 2.4

$$[e_{aq}^-]_t = \left(\frac{\Phi_{e_{aq}^-}I_0(1 - 10^{-(\varepsilon_{sens}[sens]_t + \alpha_t)l})}{\sum_i k_{S_i,e_{aq}^-}[S_i]_t}\right)\left(\frac{\varepsilon_{sens}[sens]_t}{l(\varepsilon_{sens}[sens]_t + \alpha_t)}\right) \tag{2.4}$$

where $\Phi_{e_{aq}^-}$ is the e_{aq}^- quantum yield of the sensitizer (sens), I_0 is the photon irradiance (mmol photons $cm^{-2}\ s^{-1}$), ε_{sens} is the molar absorption coefficient $(M^{-1}\ cm^{-1})$ of the sensitizer, $[sens]_t$ is the sensitizer's concentration at time t (M), α_t is the absorption of the background water matrix (cm^{-1}) at time t, k_{S_i,e_{aq}^-} is the bimolecular reaction rate constant for transformation of scavenger S_i $(M^{-1}\ s^{-1})$, $[S_i]_t$ is the scavenger concentration (M) at time t, and l is the path length (cm).[41] The units in eq 2.4 are consistent because the conversion from mmol to mol and cm^3 to L cancel each other.[41]

Integrating eq 2.1 results in a complete expression (eq 2.5), which can be employed to model the change in $[TC]$ as a function of time.

$$\ln\left(\frac{[TC]_t}{[TC]_0}\right) = -\left(k'_d t + k_{TC,e_{aq}^-}\int_0^t [e_{aq}^-]_t dt\right)$$

$$(2.5)$$

In eq 2.5, $\int_0^t [e_{aq}^-]_t \, dt$ is called the e_{aq}^- exposure and incorporates both $R_{f,t}^{e_{aq}^-}$ and $k'_{S,t}$ for any given background water matrix conditions. While the above expressions are time-based, it is also possible to present target contaminant transformation kinetics using fluence-based rate constants, which has been discussed extensively by Bolton et al.[42]

Direct photolysis plays a minor but non-negligible role in the transformation of some target contaminants. The contribution of direct photolysis to contaminant transformation in UV-ARP can be calculated in terms of the direct photolysis rate constant, k'_d

$$k'_d = \Phi_{TC}\frac{I_0}{l}(1 - 10^{-(\varepsilon_{TC}[TC]_t + \alpha_t)l})\left(\frac{\varepsilon_{TC}}{\varepsilon_{TC}[TC]_t + \alpha_t}\right)$$

$$(2.6)$$

where Φ_{TC} is the reaction quantum yield for direct photolysis of the TC, ε_{TC} is the molar absorption coefficient of the TC (M^{-1} cm^{-1}), and other terms ($[TC]$, I_0, l, and α_t) are as defined previously.[41] A key point is that there must be overlap between the spectra of the light source and TC for direct photolysis to occur (Grotthus−Draper law[43]). Contaminants containing chromophores that absorb in the UVC (e.g., nitrate, nitrite, and halogenated aromatic compounds) undergo direct photolysis.[44−46] Given the typical minor role of direct photolysis in UV-ARP, the factors influencing this pathway are not discussed extensively in this Review. Section 3 will specify contaminant classes in which direct photolysis plays a role.

2.2. Kinetics of Hydrated Electron Scavenging Reactions

Background water matrix components that react with e_{aq}^- decrease its availability for reaction with the target contaminant (TC) according to the following competition

$$TC + e_{aq}^- \rightarrow products \qquad (2.7)$$

$$S + e_{aq}^- \rightarrow products \qquad (2.8)$$

where S represents the sum of e_{aq}^- scavengers other than the TC. The expected impact of e_{aq}^- scavengers on target contaminant transformation can be estimated by determining the first-order scavenging capacity ($k'_{S,t}$, s^{-1}), which is defined as the sum product of bimolecular e_{aq}^- scavenging rate constants (k_{S_i,e_{aq}^-}) and $[S_i]_t$ (eq 2.9)

$$k'_{S,t} = \sum_i k_{S_i,e_{aq}^-}[S_i]_t$$

$$(2.9)$$

Bimolecular rate constants for e_{aq}^- reactions depend on temperature and aqueous ionic strength according to the Arrhenius (eq 2.10) and Brønsted−Bjerrum equations (eq 2.11), respectively.[8]

$$\ln\left(\frac{k_{2,T_2}}{k_{2,T_1}}\right) = \frac{E_a(T_2 - T_1)}{RT_1T_2}$$

$$(2.10)$$

$$\log\left(\frac{k_{2,I}}{k_{2,I=0}}\right) = 1.02Z_A Z_B \frac{\sqrt{I}}{1 + \sqrt{I}}$$

$$(2.11)$$

In these equations, k_2 represents the bimolecular rate constant at two different temperatures (T_1 or T_2, units of K) or ionic

strengths ($I = 0$ or I, units of M), E_a is the activation energy (kJ/ mol), R is the gas constant, and $Z_A Z_B$ is the product of the charges of the reactants. Because e_{aq}^- bears a negative charge, its reactivity with anionic species will be enhanced at higher ionic strengths because the increased shielding of like-charged reactants decreases the distance over which Coulombic forces repel the ions. Many of the contaminant classes highlighted in this Review are anionic at pH ranges used for UV-ARP, so increasing ionic strength will increase the e_{aq}^- bimolecular rate constant.

Figure 3 shows the relative change in the e_{aq}^- bimolecular rate constant as a function of temperature (10−40 °C) and ionic
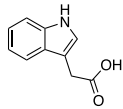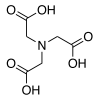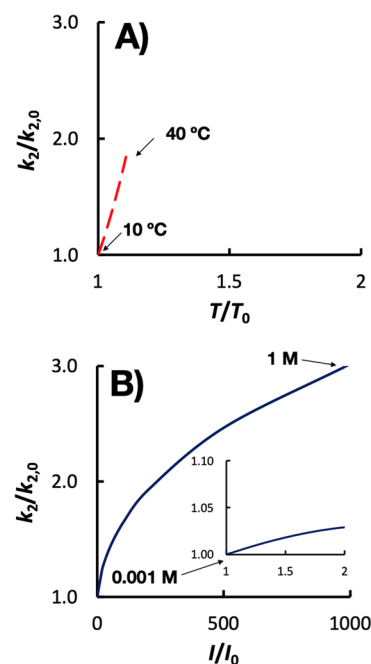
Figure 3. Relative change in bimolecular rate constant (k_2) as a function of the relative change in A) temperature (T) or B) ionic strength (I). Note the difference in scale of the x axis. The temperature dependence calculation assumes an activation energy of 15 kJ/mol, which is typical for radical reactions. The ionic strength dependence calculation assumes that $Z_A Z_B = 1$ as this would cause an increase in k_2 with increasing ionic strength. The inset in (B) has the same axes labels as the outer figure.

strength (0.001−1 M), which covers the range of values that could be anticipated in waters treated by UV-ARP. An activation energy of 15 kJ/mol and $Z_A Z_B$ of 1 were assumed for these calculations. The bimolecular rate constant is more sensitive to temperature than ionic strength, with much higher ionic strengths (hundreds of mol/L) needed to achieve the same impact on the rate constant as a 10−40 °C temperature increase. Treatment processes that concentrate contaminants (e.g., by filtration or ion exchange) prior to UV-ARP readily achieve high ionic strengths. Thus, bimolecular rate constants will need to be modified accordingly (eq 2.11) when applying quantitative kinetic models (e.g., eq 2.5) in these high ionic strength systems.

2.2.1. Hydrated Electron Scavenging Reactions in Real-World Waters. In UV-ARP systems, there are many e_{aq}^- scavengers, all with varying concentrations and reactivities toward e_{aq}^-. Scavengers can arise from background water matrix components (H^+, O_2, NO_3^-, NO_2^-, and DOM) and even the e_{aq}^- sensitizer itself (see section 2.3). A list of e_{aq}^- bimolecular rate

Table 1. Bimolecular Rate Constants for Reaction of e_{aq}^- with Species Discussed in This Review[a]

Name	Formula/Structure	Reaction	Bimolecular rate constant, k ($M^{-1}s^{-1}$)	Comment
Proton	H^+	$H^+ + e_{aq}^- \rightarrow H^\bullet$	2.3×10^{10}	Listed value is from Buxton *et al.* compilation.[8] The NDRL/NIST website has 19 entries, most ~2×10^{10} $M^{-1}s^{-1}$.
Oxygen	O_2	$O_2 + e_{aq}^- \rightarrow O_2^{\bullet-}$	1.9×10^{10}	Listed value is from Buxton *et al.* compilation.[8] Values in NDRL/NIST database range from 1.8 to 2.2×10^{10} $M^{-1}s^{-1}$.
Nitrate	NO_3^-	$NO_3^- + e_{aq}^- \rightarrow NO_3^{2-}$	9.7×10^9	Listed value is from Buxton *et al.* compilation.[8] Values in NDRL/NIST database range from 0.66 to 1.1×10^{10} $M^{-1}s^{-1}$.
Nitrite	NO_2^-	$NO_2^- + e_{aq}^- \rightarrow NO_2^{2-}$	3.5×10^9	Listed value is most recent measurement. Values in NDRL/NIST database range from 3.4 to 4.6×10^9 $M^{-1}s^{-1}$.
Nitrous oxide	N_2O	$N_2O + e_{aq}^- \rightarrow N_2 + O^{\bullet-}$	9.1×10^9	N_2O is used in some UV-ARP literature to verify the role of e_{aq}^- in target contaminant transformation. pK_a of $^\bullet OH$ is 11.9.[8]
Bicarbonate	HCO_3^-	$HCO_3^- + e_{aq}^- \rightarrow H^\bullet + CO_3^{2-}$	$<1 \times 10^6$	Value is an upper limit.
Carbonate	CO_3^{2-}	$CO_3^{2-} + e_{aq}^- \rightarrow$ products	3.9×10^5	Value derived from intercept of plots of bimolecular rate constant versus [U(VI)] [47].
Dissolved organic matter	DOM	$DOM + e_{aq}^- \rightarrow$ products	-	Value unknown, but expected to be ~10^8 L molC^{-1} s^{-1} based on DOM reactivity with $^\bullet OH$.
Sulfite	SO_3^{2-}	$SO_3^{2-} + e_{aq}^- \rightarrow$ products	$<1.5 \times 10^6$	Value is an upper limit.
Bisulfite	HSO_3^-	$HSO_3^- + e_{aq}^- \rightarrow H^\bullet + SO_3^{2-}$	1.2×10^8	From laser flash photolysis measurements [48]. Unclear how or if authors corrected for ionic strength.
Iodide	I^-	$I^- + e_{aq}^- \rightarrow$ products	$<2.4 \times 10^5$	Value is an upper limit.
Iodine	I_2	$I_2 + e_{aq}^- \rightarrow I_2^{\bullet-}$	5.6×10^{10}	I_2 is formed during photolysis of iodide
Triiodide	I_3^-	$I_3^- + e_{aq}^- \rightarrow I_2^{\bullet-} + I^-$	3.5×10^{10}	Triiodide is formed during photolysis of iodide
Iodine radical anion	$I_2^{\bullet-}$	$I_2^{\bullet-} + e_{aq}^- \rightarrow$ products	9×10^{10}	Derived from fitting complex reaction mechanism with multiple assumptions. Accuracy is circumspect.
3-Indoleacetic acid (IAA)		$IAA + e_{aq}^- \rightarrow$ products	1.7×10^8	From ref. [49] measured at pH 11; two values listed in NDRL/NIST data base are for indole and are 2.6 and 1.9×10^8 $M^{-1}s^{-1}$.
Nitrilotriacetic acid (NTA)		$NTA + e_{aq}^- \rightarrow$ products	0.3 to 3.6×10^7	Values derived from intercept of plots of bimolecular rate constant versus [U(VI)]. The range of values represents different initial NTA concentrations (0.01 to 0.25 M) and pH values (9.0 and 9.5) [47].
Bromate	BrO_3^-	$BrO_3^- + e_{aq}^- \rightarrow BrO_3^{2-}$	2.3×10^9	pH 13, ionic strength → 0. Values for BrO_2^- and BrO^- (pH 13, ionic strength → 0) are 11×10^9 and 15×10^9 $M^{-1}s^{-1}$, respectively.
Perchlorate	ClO_4^-	$ClO_4^- + e_{aq}^- \rightarrow$ products	$<1 \times 10^6$	Value is an upper limit. Values for ClO_3^-, ClO_2^-, and ClO^- are $<1.6 \times 10^6$, 2.5×10^9 (pH 10), and 7.3×10^9 $M^{-1}s^{-1}$ (pH 9.2, ionic strength → 0), respectively.
Chloroacetate	$ClCH_2COO^-$	$ClCH_2COO^- + e_{aq}^- \rightarrow$ $^\bullet CH_2COO^- + Cl^-$	1.0×10^9	Value for protonated species is 6.9×10^9.
Fluoroacetate	FCH_2COO^-	$FCH_2COO^- + e_{aq}^- \rightarrow$ products	$<1.2 \times 10^6$	Value is an upper limit.

[a]Values obtained from the NDRL/NIST solution kinetics database (https://kinetics.nist.gov/solution/) unless otherwise noted. The reaction products are shown only if present in the NDRL/NIST database. See Table 4 for tabulated e_{aq}^- bimolecular rate constants for PFAS. The Supporting Information contains a larger list of e_{aq}^- bimolecular rate constants for aliphatic and aromatic compounds.

constants used extensively in this Review is provided in Table 1. This list does not describe all e_{aq}^- reactions or those initiated by

e_{aq}^- that could be occurring in UV-ARP. We refer readers to the Notre Dame Radiation Laboratory/National Institute of

Standards and Technology solution kinetics database (https://kinetics.nist.gov/solution/) as a source of bimolecular rate constants for e_{aq}^- and other radical species.

From, eq 2.4, we can see that $[e_{aq}^-]$ is inversely proportional to $k'_{S,t}$. In principle, it is possible to calculate $k'_{S,t}$ a priori provided the concentrations and rate constants for all important e_{aq}^- scavengers are known. Figure 4 illustrates this fact by showing
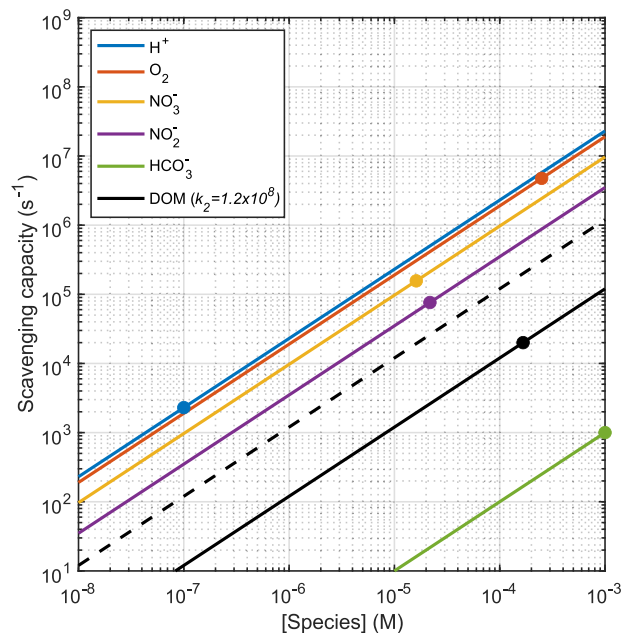
$[O_2] = 250\ \mu M$) if not removed prior to treatment, which is an important limitation of UV-ARP (see section 2.2.2). Nitrate is a potent e_{aq}^- scavenger, and the concentration of this species in natural waters (~ 1 mg/L for 50% of natural waters in the United States[52]) will exert a significant scavenging capacity ($k'_{S,t=0} = 2.02 \times 10^5\ s^{-1}$), thus limiting the effectiveness of UV-ARP. This idea is illustrated by Figure 5 which shows that UV/sulfite treatment

Figure 4. Scavenging capacities of ($k'_{S,t=0}$) as a function of species concentration for some e_{aq}^- scavengers in UV-ARP. Bimolecular rate constants used for these calculations are shown in Table 1. A value of $1.2 \times 10^8\ M_C^{-1}\ s^{-1}$ ($\sim 10^4$ L mgC^{-1} s^{-1}) was used for the DOM-e_{aq}^- reaction based on the DOM-$^\bullet$OH rate constant for SRFA.[50] Filled circles represent the scavenging capacity of each species under the following conditions: $[H^+] = 10^{-7}$ M, $[O_2] = 250 \times 10^{-6}$ M (8 mg/L), $[NO_3^-] = 1.61 \times 10^{-5}$ M (1 mg/L), $[NO_2^-] = 2.17 \times 10^{-5}$ M (1 mg/L), $[DOM] = 1.66 \times 10^{-4}$ molC L^{-1} (2 mgC/L), and $[HCO_3^-] = 10^{-3}$ M (61 mg/L).

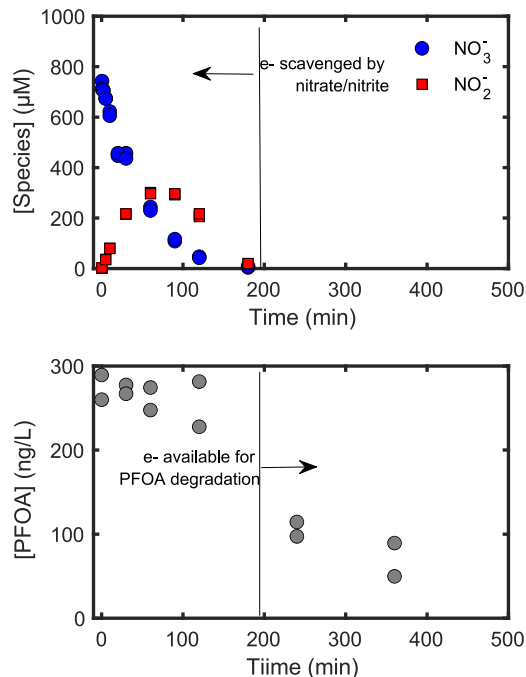**Figure 5.** Time courses of nitrate, nitrite, and perfluorooctanoic acid (PFOA) during UV/sulfite treatment of a contaminated groundwater. Line at ~ 200 min illustrates the point at which e_{aq}^- scavenging by the water matrix becomes low enough for PFOA-e_{aq}^- reactions to occur. Experimental conditions: 18 W low-pressure Hg lamp, pH$_0$ = 9.5, 10 mM sulfite, 30 min of sparging with industrial grade N$_2$, ACE glass water-jacketed immersion well reactors. PFOA concentration was measured according to previously described literature methods.[32]

the scavenging capacity for selected water matrix components as a function of their concentration (eq 2.9) calculated using the values in Table 1. While bimolecular e_{aq}^- rate constants are widely available for important hydrated electron scavengers,[8] conducting a full water chemistry analysis to determine scavengers' concentrations is not always practical. In addition, Rosenfeldt and Linden demonstrated that calculated $^\bullet$OH scavenging capacities in UV-AOP differed substantially from values measured with *p*-chlorobenzoic acid,[40] suggesting that the same may be true for UV-ARP.

These scavenging capacities allow for comparison of the impact of different water matrix components on $[e_{aq}^-]$. For example, while the fastest bimolecular rate constant is for e_{aq}^- reaction with H$^+$, the typical $[H^+]$ (pH > 9) is optimized to minimize this pathway, making the e_{aq}^- scavenging capacity of H$^+$ a small contribution to $k'_{S,t}$ in most UV-ARP.[48] Dissolved oxygen ($\sim 250\ \mu M$ in aerated water) is a significant scavenger of e_{aq}^-. In UV-ARP treatment, removal of dissolved oxygen is accomplished through mechanical deaeration (sparging with N$_2$ or Ar) or reactive quenching by sulfite,[32,51] which also functions as an e_{aq}^- sensitizer. Figure 4 demonstrates that dissolved oxygen will exert a significant scavenging capacity ($k'_{S,t=0} = 4.75 \times 10^6\ s^{-1}$ for

of perfluorooctanoic acid (PFOA) in a contaminated groundwater is limited until nearly all nitrate and nitrite (formed during nitrate photoreduction) have been degraded.

Another probable e_{aq}^- scavenger is dissolved organic matter (DOM). Despite the ubiquity of DOM in waste streams for UV-ARP treatment, the reactivity between e_{aq}^- and DOM remains unexplored. DOM contains several oxygenated functional groups,[53] which, as individual chemical moieties, are known to have high reactivity with e_{aq}^-. These moieties include carbonyl-containing compounds (e.g., aldehydes, ketones, and quinones), alkoxyphenols, and amino acids.[8,54] The estimated value of 10^4 L mgC^{-1} s^{-1} ($\sim 10^8$ L molC^{-1} s^{-1}) shown in Table 1 is based on the bimolecular rate constant for the reaction between DOM isolates and the hydroxyl radical reported by Westerhoff et al.[50]

2.2.2. Hydrated Electron Scavenging by Dissolved Oxygen in Laboratory Studies. UV-ARP studies are often performed in buffered, laboratory grade water that has been sparged with an inert gas like nitrogen to remove dissolved O$_2$. However, prior research shows that a residual $[O_2]$ of approximately 0.2 mg/L ($\sim 6\ \mu M$) remains even after sparging with nitrogen (25 mL/s) for 1 h.[55] An $[O_2]$ of 6 μM in deaerated solutions will still exhibit a high e_{aq}^- scavenging capacity ($k'_{S,t=0} = 1.2 \times 10^5\ s^{-1}$), which will impact the initial $[e_{aq}^-]$ and thereby the

rate of target contaminant transformation. Therefore, variations in $[O_2]$ in laboratory studies with different sparging methods may substantially impact the observed kinetics for target contaminant transformation, making it difficult to compare UV-ARP data for different sensitizer systems and experimental setups. In addition, the use of different e_{aq}^- sensitizers may impact the residual $[O_2]$ since reducing species like sulfite can remove O_2.[32,51]

The impact of residual $[O_2]$ will also depend on the solution conditions and target contaminant. Residual $[O_2]$ will have the largest impact on the degradation of contaminants that have an e_{aq}^- bimolecular rate constant comparable to O_2 and thus react on similar time scales. Examples include nitrate, nitrite, and most halogenated organic compounds. On the other hand, target contaminants with slower e_{aq}^- bimolecular rate constants will be less impacted because the residual $[O_2]$ will be reduced by e_{aq}^- at early reaction times. For example, Bentel et al. observed similar degradation kinetics for PFOA in the UV/sulfite system regardless of whether the solution was initially sparged with nitrogen.[30] This concept is further illustrated in Figure 6, which
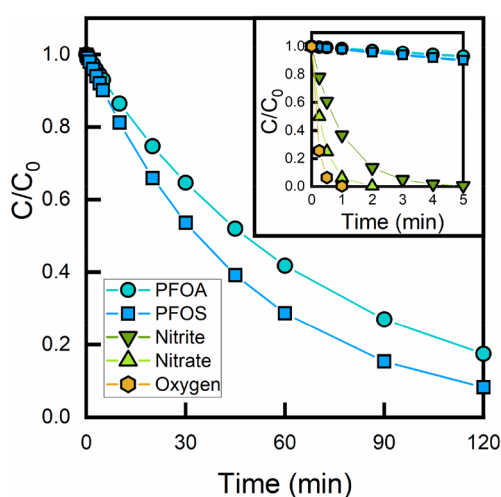

Figure 6. Calculated concentration profiles of typical UV-ARP target contaminants based on eq 2.5, assuming $[e_{aq}^-] = 4.76 \times 10^{-12}$ M, direct photolysis for nitrate and nitrite, and bimolecular rate constants $(M^{-1} s^{-1})$ of $k_{PFOA,e_{aq}^-} = 5.1 \times 10^7$, $k_{PFOS,e_{aq}^-} = 7.3 \times 10^7$, $k_{NO_3^-,e_{aq}^-} = 9.7 \times 10^9$ $M^{-1} s^{-1}$, $k_{NO_2^-,e_{aq}^-} = 3.5 \times 10^9$ $M^{-1} s^{-1}$, $k_{O_2,e_{aq}^-} = 1.9 \times 10^{10}$ $M^{-1} s^{-1}$.

shows the calculated concentration profiles for the transformation of several compounds in a typical UV-ARP. Fast-reacting compounds like oxygen, nitrate, and nitrite are completely removed within a few minutes, while perfluorooctanoic acid (PFOA) and perfluoroctanesulfonate (PFOS), two representative PFAS, are degraded at much longer time scales.

2.3. Chemical Sensitizers for Hydrated Electron Production

It is possible to generate e_{aq}^- from the photolysis of many organic and inorganic compounds if the appropriate illumination wavelengths are used.[56] However, only a subset of the chemicals capable of producing e_{aq}^- under UV irradiation have been explored in UV-ARP. Absorption of photons by sensitizer (sens) molecules will result in a portion of them ejecting an electron (eq 2.12).[56]

$$sens^n + h\nu \rightarrow sens^{n+1} + e^- \qquad (2.12)$$
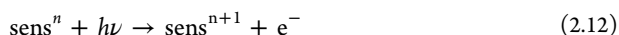
The ejected e^- initially forms an ion contact pair with $sens^{n+1}$, and only a fraction of e^- eventually escapes the contact pair to

form hydrated electrons, e_{aq}^-. The overall efficiency of this process can be described by the quantum yield of e_{aq}^- formation $(\Phi_{e_{aq}^-})$, which represents the rate of e_{aq}^- formation $(R_f^{e_{aq}^-}, M s^{-1})$ divided by the rate of light absorption by the sensitizer (photons $L^{-1} s^{-1}$). Employing sensitizers with higher $\Phi_{e_{aq}^-}$ therefore represents one possible approach to enhancing $[e_{aq}^-]$ in UV-ARP. The UV photochemistry of many of these e_{aq}^- sensitizers was recently reviewed by Cui et al.[2]

Table 2 provides a summary of e_{aq}^- sensitizers that have been examined in the literature, their molar absorption coefficient (ϵ) at selected wavelengths, $\Phi_{e_{aq}^-}$ values, and the method of $\Phi_{e_{aq}^-}$ determination. There is some variation in ϵ and $\Phi_{e_{aq}^-}$ and some sensitizers for which no data are available. Reported $\Phi_{e_{aq}^-}$ values for sulfite vary by less than a factor of 2. The $\Phi_{e_{aq}^-}$ value of 0.116 at 254 nm determined by steady-state photolysis[57] is in good agreement with the recent value of 0.108 at 248 nm measured by transient absorption spectroscopy.[48] Given the agreement between these two values, we expect that a $\Phi_{e_{aq}^-}$ of ≈ 0.1 for sulfite is reliable. Uncertainty in $\Phi_{e_{aq}^-}$ values impact the ability of kinetic models to accurately predict the change in $[TC]$ with time according to eq 2.5.

To help address the uncertainty in ϵ_{254} values, we have measured molar absorption coefficients for 3-indoleacetic acid (IAA), nitrilotriacetic acid (NTA), iodide, and sulfite (Figure 7), four of the e_{aq}^- sensitizers employed most frequently in UV-ARP studies. Our results agree well with most with literature data, where available. For sulfite, ϵ_{254} values agree within ~15%, and we suggest that the value measured by Tenorio et al. (17.8 $M^{-1}cm^{-1}$) is reliable.[34] Our measured ϵ_{254} for iodide (172 $M^{-1}cm^{-1}$) agrees well with one literature report (162 $M^{-1}cm^{-1}$)[61] but is substantially different from another (220 $M^{-1}cm^{-1}$).[60]

2.3.1. Sulfite. Sulfite is one of the most studied e_{aq}^- sensitizers in UV-ARP systems. Sulfite absorbs in the UV region of the spectrum $(\epsilon_{254} \approx 18 \, M^{-1}cm^{-1})$[57] and its $\Phi_{e_{aq}^-}$ has been measured in several previous studies.[48,57,68]

$$SO_3^{2-} + h\nu \rightarrow SO_3^{\bullet -} + e_{aq}^- \qquad \Phi_{e_{aq}} = 0.108-0.174$$

$$(2.13)$$
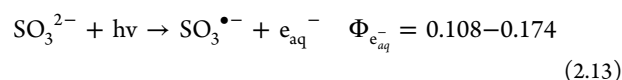
In the absence of oxygen, dithionate $(S_2O_6^{2-})$ and sulfate are the major end products of this reaction, while in oxygenated solutions only sulfate is observed.[68]

e_{aq}^- generation in the UV/sulfite ARP is much less efficient at pH values near and below the pK_a of HSO_3^- (7.19) because photolysis of HSO_3^- has a low $\Phi_{e_{aq}^-}$.[69] In addition, HSO_3^- is a scavenger of e_{aq}^-.[48]

$$HSO_3^- + e_{aq}^- \rightarrow {}^\bullet H + SO_3^{2-} \qquad k = 1.2 \times 10^8 \, M^{-1} s^{-1}$$

$$(2.14)$$
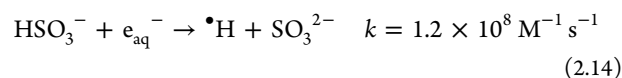
Moreover, sulfite itself reacts with e_{aq}^-. Although the SO_3^{2-}-e_{aq}^- reaction is slow (the upper limit for the rate constant is 1.6×10^6 $M^{-1} s^{-1}$),[8] the high sulfite concentrations typically employed in UV-ARP (ca. 10 mM) could mean that this reaction pathway is significant. For example, Figure 8 shows the calculated e_{aq}^- formation rate $(R_f^{e_{aq}^-})$, scavenging capacity $(k'_{S,t=0})$, and $[e_{aq}^-]$ expected in an aqueous solution containing monochloroacetate (MCAA at a fixed concentration of 20 μM) and sulfite at various concentrations (between 0 and 20 mM). The e_{aq}^- scavenging capacity exerted by sulfite increases linearly with increasing

Table 2. Summary of Hydrated Electron (e_{aq}^-) Sensitizers Used in UV-ARP, Their Quantum Yields ($\Phi_{e_{aq}^-}$), and the Method of $\Phi_{e_{aq}^-}$ Determination if Available

Sensitizer [a]	Formula or structure	ϵ (M^{-1}cm^{-1}) (wavelength)	$\Phi_{e_{aq}^-}$ (wavelength) [f]	Method of determination
Iodide [1, 58]	I$^-$	885 (248 nm) [59] 220 (254 nm) [60] 162 (254) [b, 61] 172 (254) [c]	0.22 (248 nm) [62] 0.286 (248 nm) [59]	Laser flash photolysis and transient absorption spectroscopy
Sulfite [16, 30, 34, 57] (pK$_{a1}$ = 1.8, pK$_{a2}$ = 7.1)	SO$_3^{2-}$	49 (248 nm) [59] 20.3 (254 nm) [63] 18.4 (254 nm) [57] 17.8 (254) [b, 34] 17.6 (254) [c]	0.174 (266 nm) [48] 0.108 (248 nm) [59] 0.116 (254 nm) [57]	Laser flash photolysis and transient absorption spectroscopy; Laser flash photolysis and transient absorption spectroscopy; Steady state photolysis of sulfite e_{aq}^- detected with chloroacetate
Sulfite/iodide [60]	See above entries	See above entries	Values for mixtures not reported	Not reported
Nitrilotriacetic acid [64] (pK$_{a1}$ = 3.03, pK$_{a2}$ = 3.07, pK$_{a3}$ = 10.7)		26.3 (254) [c]	Not reported	Not reported
Indole-3-acetic acid (pK$_a$ = 4.7) + derivatives [25, 26, 64, 65]		3400 (254) [d, 66] 2576 (254) [c]	0.14 (254 nm) [e, 67]	Steady state photolysis of indole; e_{aq}^- quantified by measuring chloride formation from 2-chloroethanol

[a]Referenced study refers to application of the sensitizer in UV-ARP systems. [b]ϵ_{254} estimated using Web Plot Digitizer (https://apps.automeris.io/wpd/). [c]Measured for this Review. [d]Value is for indole (not indoleacetic acid) in ethanol. [e]Value is for indole (not indoleacetic acid) at 30 °C. [f]Measurements are conducted in deaerated solutions.
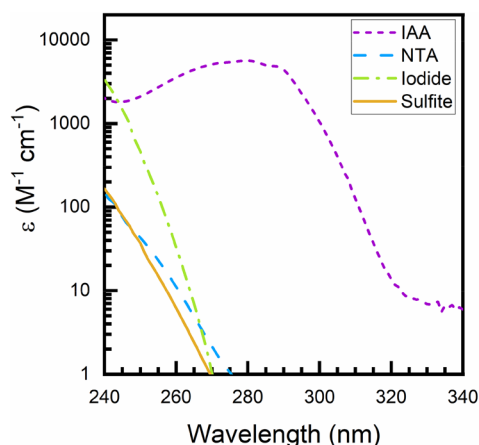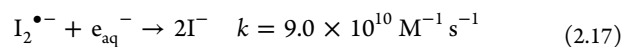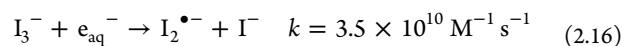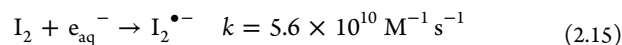

Figure 7. Absorption spectra for four commonly used hydrated electron sensitizers in UV-ARP studies, including 3-indoleacetic acid (IAA), nitrilotriacetic acid (NTA), iodide, and sulfite. Molar absorption coefficients at 254 nm (ϵ_{254}) are 17.6 M^{-1}cm^{-1} (sulfite), 26.3 M^{-1}cm^{-1} (NTA), 172 M^{-1}cm^{-1} (iodide), and 2576 M^{-1}cm^{-1} (IAA) and are listed in Table 2. Experimental conditions: All solutions besides iodide (potassium iodide) were prepared in pH 10 borate buffer (10 mM), whereas potassium iodide was prepared in unbuffered laboratory grade water (18.2 MΩ·cm). Sulfite solutions were prepared in N$_2$ sparged (30 min) water. Molar absorption coefficients are derived from a linear fit of absorbance to molar concentration with an absorbance (optical density) less than 2.0 measured with a Cary-100 Bio dual beam spectrophotometer in a 1 cm path length quartz cuvette.
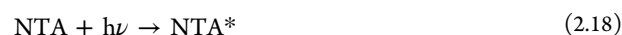
sulfite concentration (eq 2.9). However, $R_f^{e_{aq}^-}$ increases asymptotically due to the $(1-10^{-(\epsilon_{sens}[sens]_t + \alpha_t)l)}$ term in eq 2.4. Overall, this results in an asymptotic increase in $[e_{aq}^-]$ with increasing sulfite concentration. Although there is not a consensus on an optimal sulfite concentration in UV-ARP, previous literature demonstrates diminishing increases in target

contaminant transformation kinetics above ∼10 mM sulfite.[13,23,34] This is consistent with the calculations presented in Figure 8.

2.3.2. Iodide. Iodide photolysis produces e_{aq}^- with a $\Phi_{e_{aq}^-}$ of ≈0.2 at 248 nm.[59] This is approximately a factor of 2 higher than the $\Phi_{e_{aq}^-}$ for sulfite. Iodide also has a higher molar absorption coefficient at 254 nm than sulfite (Table 2). However, as will be discussed further below, several UV-ARP studies have demonstrated that target contaminant transformation rates are faster in the UV/sulfite system compared to the UV/iodide system. This indicates that the $[e_{aq}^-]$ is higher in the UV/sulfite system, despite iodide's higher $\Phi_{e_{aq}^-}$ and ϵ_{254} values. The lower $[e_{aq}^-]$ in the UV/iodide system is likely due to e_{aq}^- scavenging reactions[70,71] of I-containing species, like iodine and triiodide, which are formed during photooxidation of iodide.

$$I_2 + e_{aq}^- \rightarrow I_2^{\bullet -} \quad k = 5.6 \times 10^{10} \text{ M}^{-1}\text{s}^{-1} \quad (2.15)$$

$$I_3^- + e_{aq}^- \rightarrow I_2^{\bullet -} + I^- \quad k = 3.5 \times 10^{10} \text{ M}^{-1}\text{s}^{-1} \quad (2.16)$$

$$I_2^{\bullet -} + e_{aq}^- \rightarrow 2I^- \quad k = 9.0 \times 10^{10} \text{ M}^{-1}\text{s}^{-1} \quad (2.17)$$

2.3.3. Nitrilotriacetic Acid. Nitrilotriacetic acid (NTA) produces e_{aq}^- at UV irradiation wavelengths, but with an unknown quantum yield. It has been proposed that the mechanism of e_{aq}^- formation from nitrilotriacetic acid photolysis does not involve photoionization of nitrilotriacetic acid (eq 2.1).[56] Instead, electronically excited nitrilotriacetic acid is thought to sensitize the photooxidation of water, concomitantly producing e_{aq}^-, $^{\bullet}$OH, and $^{\bullet}$H.[56,64]

$$NTA + h\nu \rightarrow NTA^* \quad (2.18)$$

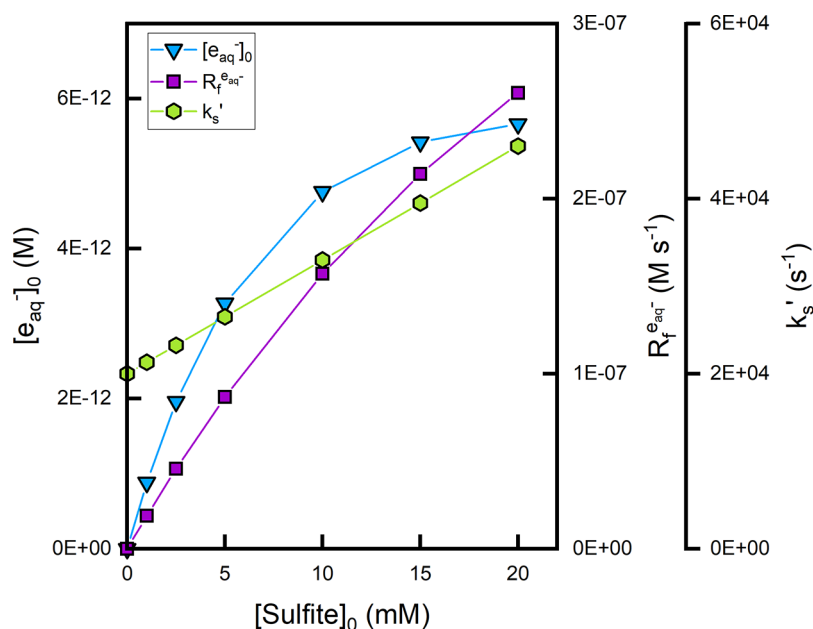$$NTA^* + H_2O \rightarrow e_{aq}^- + {}^{\bullet}OH + H^+ + NTA \quad (2.19)$$

Figure 8. Plot of calculated e_{aq}^- formation rate ($R_{f,t=0}^{e_{aq}^-}$), scavenging capacity ($k_{S,t=0}'$), and $[e_{aq}^-]_{t=0}$ ($\frac{R_f^{e_{aq}^-}}{k_{S,t=0}'}$) as a function of initial sulfite concentration. It is assumed that sulfite functions as the sole light absorber while both sulfite and another target compound (MCAA) act as e_{aq}^- scavengers. Conditions: $I_0 = 1.13 \times 10^{-8}$ Es cm^{-2} s^{-1}, $\Phi_{e_{aq}^-} = 0.116$ mol Es^{-1}, $\varepsilon_{sens} = 18.14$ M^{-1} cm^{-1}, $l = 2.85$ cm, $k_{sulfite,e_{aq}^-} = 1.3 \times 10^6$ M^{-1} s^{-1}, $k_{MCAA,e_{aq}^-} = 1.0 \times 10^9$ M^{-1} s^{-1}, $[MCAA]_0 = 20$ μM, pH$_0$ = 9.5.

Photoproduced $^\bullet$OH can react with the C−H bonds in nitrilotriacetic acid through H atom abstraction (eq 2.20),[64]

$$NTA + {}^\bullet OH \rightarrow products$$
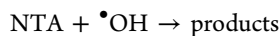
$$k = 4.2 \times 10^9 \text{ M}^{-1}\text{ s}^{-1} \text{ (pH 10)} \qquad (2.20)$$

which reduces the $^\bullet$OH-e_{aq}^- recombination rate ($k = 2.8 \times 10^{10}$ M^{-1} s^{-1})[72] thereby allowing more e_{aq}^- to react with target contaminants.

Historically, the mechanism proposed for nitrilotriacetic acid is an alternative to the photooxidation mechanism previously described (eq 2.12) and may in fact be operative for other e_{aq}^- sensitizers. The main point is that both mechanisms (photoionization and NTA-sensitized H$_2$O ionization) yield e_{aq}^-.

2.3.4. Indole derivatives. It has been suggested that indoles produce e_{aq}^- through the photoionization mechanism described in eq 2.12 with $\Phi_{e_{aq}^-}$ of ≈0.1 (Table 2). Given the high molar absorption coefficient of 3-indoleacetic acid at 254 nm (≈ 2600 M^{-1} cm^{-1}) and $\Phi_{e_{aq}^-}$ value comparable to that of sulfite, indoles should have high rates of e_{aq}^- formation in UV-ARP systems. However, previous studies of UV/indoleacetic acid treatment of PFOA show no difference in degradation rates between direct photolysis controls and in the presence of 1 mM 3-indoleacetic acid.[25] This observation could indicate a high rate of scavenging between e_{aq}^- and indole itself ($k = 2.6 \times 10^8$ M^{-1} s^{-1})[49] or indole photoproducts that limits the $[e_{aq}^-]$ available for reaction with PFOA. As discussed later (see Section 3.2.3), indoleacetic acid does effectively defluorinate PFOA in a heterogeneous UV-ARP involving an organomontmorillonite clay surface.[25,26]

2.3.5. Vacuum UV. An alternative to the use of e_{aq}^- sensitizers is vacuum UV photons (VUV, 100 nm < λ < 200 nm), which are capable of directly ionizing water molecules to form e_{aq}^-, H$^\bullet$, and $^\bullet$OH.[73] For example, studies have shown that photolysis of aqueous PFAS with Hg lamps not manufactured to block VUV

degrades these contaminants in the absence of any added e_{aq}^- sensitizer,[24,74] implying that photoionization of water by the small amount of VUV emitted from these lamps is occurring. Practically, VUV is challenging to implement, as VUV photons are absorbed within the first ~5 mm of water.[73]

2.3.6. Factors Influencing the Choice of Chemical Sensitizer. Several studies have attempted to optimize experimental conditions to maximize the rate of e_{aq}^- generation from these sensitizers. For example, Yu et al. demonstrated that reductive dechlorination of monochloroacetate in the UV/ iodide system is enhanced by adding sulfite.[60] In this case, it is believed that sulfite reduces reactive iodine species (e.g., I$_2$, I$_3^-$) back to iodide, whereas in the absence of sulfite, these reactive iodine species significantly scavenge e_{aq}^- (eqs 2.15−2.17). In the Yu et al. study, monochloroacetate dechlorination was fastest in the UV/sulfite/iodide system, when compared to UV/iodide and UV/sulfite.[60] Similarly, Sun et al. observed faster degradation of perfluorooctanesulfonate by UV/nitrilotriacetic acid when compared to UV/sulfite.[64] In this case, nitrilotriacetic acid was hypothesized to concomitantly sensitize the formation of e_{aq}^- and scavenge photoproduced $^\bullet$OH (eq 2.18−2.20).

Another important aspect of selecting an e_{aq}^- sensitizer for UV-ARP is the sensitizer's expected degradation products. For example, iodide photolysis generates iodine and triiodide,[75] which absorb light in the visible region of the spectrum. These iodine species would need to be removed (e.g., through reduction to iodide) after the UV-ARP. Photolysis of nitrilotriacetic acid produces a foul odor characteristic of amine compounds.[32] Conversely, sulfite photooxidation produces inert sulfate. Although high concentrations of sulfate in drinking water should be avoided,[76] this anion is relatively benign compared to iodide and nitrilotriacetic acid photolysis products. Another benefit to using sulfite is that it can be regenerated following its oxidation to SO$_3^{\bullet-}$. This is inferred from the fact that sulfite persists in UV-ARP systems remain high even after

many hours of light exposure.[34] Conversely, when used alone, sensitizers like iodide and nitrilotriacetic acid are degraded quickly.[64]

Collectively, sensitizer concentration, e_{aq}^- quantum yield, and molar absorption coefficient at the actinic wavelength employed all impact the rate of e_{aq}^- formation and are important for sensitizer selection in UV-ARP. Byproducts of e_{aq}^- sensitizer photolysis are also an important consideration. Taken as a whole, using sulfite as a sensitizer in UV-ARP appears to have the optimal benefits for treatment applications.

2.4. Knowledge Gaps

Recent UV-ARP studies have employed an array of e_{aq}^- sensitizers, varying intensity UV light sources,[77,78] and optimized solution conditions[79] in an attempt to enhance degradation rates of target contaminants. However, progress in UV-ARP research has been limited by the lack of a systematic framework for evaluating treatment performance between these individual studies and the effect of process variables such as the UV-ARP irradiation source, sensitizer identity and concentration, and water quality. Overall, there is a need for the development of quantitative tools to allow comparison between UV-ARP studies, such as methods for quantifying $[e_{aq}^-]$ and modeling target contaminant degradation kinetics.

2.4.1. Probe Compounds for Studying UV-ARP. There is
a need to apply e_{aq}^- probe compounds to quantify photochemical parameters related to UV-ARP systems. Although several e_{aq}^- probes have been used in the broader chemical literature (vide infra), and some have been applied in UV-ARP studies, they have not been used extensively to quantify e_{aq}^- formation rates $(R_{e_{aq}^-}^f)$, e_{aq}^- concentrations $([e_{aq}^-])$, or e_{aq}^- scavenging capacities $(k_{S,t}')$ in UV-ARP. This contrasts with research on UV-AOP, which has made extensive use of p-chlorobenzoic acid as an $^\bullet$OH probe,[40,80,81] allowing for a comparisons of treatment performance.[82−85] When measured using a validated probe compound, $R_f^{e_{aq}^-}$, $[e_{aq}^-]$, and $k_{S,t}'$ provide metrics for assessing the effects of different water matrices, solution conditions, and process variables on UV-ARP treatment performance.

e_{aq}^- probe compounds used in the literature include chloroacetate (monitoring the [parent] by ion chromatography or gas chromatography),[57] chloroethanol (monitoring the product $[Cl^-]$ by ion chromatography or an ion selective electrode),[86] nitrous oxide (monitoring the $[N_2]$ by gas chromatography), and 3-amino-2,2,5,5-tetramethyl-1-pyrrolidinyloxy (monitoring the derivatized reaction product).[87]

Chloroethanol[86] and the nitroxide probe[87] were used for characterizing e_{aq}^- formation from chromophoric dissolved organic matter at UV−B and UV-A wavelengths. However, to be a successful e_{aq}^- probe in UV-ARP, the nitroxide would need to be stable under UV−C irradiation (e.g., at 254 nm, where the nitroxide is highly absorbing). Another issue with the nitroxide probe is that it requires millimolar concentrations of dimethyl sulfoxide, which absorbs at 254 nm. For these reasons it is unlikely that the nitroxide probe is suitable for quantifying $[e_{aq}^-]$ in UV-ARP. Because chloroethanol relies on measurement of $[Cl^-]$, which has a high background concentration in real-world waters, it is also unsuitable for quantifying $[e_{aq}^-]$ in UV-ARP. However, chloroethanol could be employed to measure fundamental photochemical parameters like $\Phi_{e_{aq}^-}$ in laboratory grade water containing low background $[Cl^-]$.

A few studies have demonstrated success using chloroacetate as an e_{aq}^- probe.[57,60,88,89] Chloroacetate can be quantified via ion chromatography in aqueous aliquots withdrawn from UV-ARP experiments down to ∼2 μM.[57] Lower concentrations can be quantified via derivatization and gas chromatography.[90] The availability of these analytical methods has important implications for the chosen probe compound concentration. If ion chromatography is the only method available, this limits the initial probe concentration to the micromolar range, where it can still exert a significant scavenging capacity in the system.

When employing chloroacetate as an e_{aq}^- probe, it is also possible to quantify chloride as an e_{aq}^- reduction product, but this would again be impractical in natural waters with high background $[Cl^-]$. Alternatively, the use of fluoroacetate as an e_{aq}^- probe would enable detection of fluoride since the fluoride concentration in natural waters is typically orders of magnitude lower than that of chloride.[52] Fluoroacetate is much less reactive with e_{aq}^- ($k \leq 1.2 \times 10^6 \text{ M}^{-1} \text{ s}^{-1}$[91]) than chloroacetate ($k = 1.0 \times 10^9 \text{ M}^{-1} \text{ s}^{-1}$). Thus, higher concentrations of fluoroacetate could be employed (aiding with detection limit issues) with minimal impacts to the natural e_{aq}^- scavenging capacity of the background water matrix. Use of fluoroacetate as an e_{aq}^- would require accurate measurement of its e_{aq}^- bimolecular rate constant (the current value is an upper limit) and the fluoride reaction yield (see Section 3.2.2).

While development of e_{aq}^- probe compounds is needed, several challenges unique to UV-ARP have made this difficult. First, many UV-ARP studies are conducted in buffered solutions of laboratory-grade water where there is minimal background scavenging of e_{aq}^-. This makes the system sensitive to potential e_{aq}^--reactive impurities like trace levels of O_2 not removed during prior deaeration.[92] Another potential challenge for a standard e_{aq}^- probe compound is the possibility that reactive species besides e_{aq}^- generated in UV-ARP systems could cause probe transformation. For example, $SO_3^{\bullet-}$ formed upon sulfite photooxidation has been reported to act as both an oxidant and reductant (see also section 3.3.2).[13] If $SO_3^{\bullet-}$ were to reduce the employed probe compound like e_{aq}^-, then the probe would not be selective. One way to overcome this challenge is to verify the selectivity of the probe using an e_{aq}^- quencher. Compounds like nitrous oxide, nitrate, and nitrite have been widely employed for this purpose in prior studies.[8,57,60] For example, N_2O reacts quickly with e_{aq}^- ($k = 9.1 \times 10^9 \text{ M}^{-1} \text{ s}^{-1}$) but not with $SO_3^{\bullet-}$ ($k < 1 \times 10^6 \text{ M}^{-1} \text{ s}^{-1}$) (Table 1 and https://kinetics.nist.gov/solution/).

2.4.2. Computer Kinetic Models. An alternative approach
for gaining a quantitative description of UV-ARP chemistry is by modeling the kinetics of the system through computer numerical integration, which has received considerable attention in UV-AOP systems.[93,94] The process involves collecting all the known reactions occurring in a system and their rate constants and inputting this information into a computer program. Free (e.g., Kinetcus[95]) and commercial programs (e.g., FACSIMILE) are available for building and running these kinetic models. If all parameters are known, running such programs to produce time profiles of target contaminants, intermediates, and reactive radicals is straightforward. Alternatively, if there are some unknown parameters (e.g., bimolecular rate constants, quantum yields) the kinetic model can be fit to a given data set to estimate the unknown parameters.[10,96] Despite the abundance of bimolecular e_{aq}^- rate constants available,[8] examples of such numerical computer models being applied in UV-ARP are limited.[60]

One potential limitation of computer kinetics models is that they may not be readily transferable across different UV-ARP.

Table 3. UV-ARP Organic and Inorganic Treatment Studies Summary[a]

ref	compound class	[compound]$_0$ (µM)	heterogeneous or homogeneous system	UV lamp	UV sensitizer	water characteristics	parent compound degradation % (time)
102	halogenated organic	10 µM trichloroacetic acid	heterogeneous (TiO$_2$)	LP-Hg 10 W	4.0 mM formate	ultrapure water (pH 6.5, 23 °C)	100% (150 min)
45	halogenated organic	10 µM 4-bromophenol	homogeneous	LP-Hg 10 W	1.0 mM sulfite	ultrapure water (pH 9.2, 20 °C)	100% (10 min)
103	halogenated organic	20 µM 1,2-dichloroethane	homogeneous	LP-Hg 36 W	1.0 mM dithionite; 1.2 mM sulfite; 0.4 mM sulfide; 4.0 mM ferrous iron	ultrapure water (pH 11, 11, 9, 9, 25 °C)	100% (varies)
104	halogenated organic	10 µM decabromodiphenyl ethers	homogeneous	LP-Xe 50 W and LED	none	reaction performed in methanol	90% (60 min)
105	halogenated organic	10 µM MCAA	homogeneous	n.r.	1.0 mM sulfite; 1.0 g L^{-1} bismuth oxyiodide	ultrapure water (pH 7; 25 °C)	100% (20 min)
57	halogenated organic	50 µM MCAA	homogeneous	LP-Hg 10 W	1.0 mM sulfite	ultrapure water (pH 9.2; 25 °C)	100% (15 min)
88	halogenated organic	50 µM MCAA	homogeneous	LP-Hg 15 W	0.2 mM phenol	ultrapure water (pH 12; 25 °C)	100% (6 min)
60	halogenated organic	50 µM MCAA	homogeneous	LP-Hg 10 W	1.0 mM sulfite; 0.1 mM iodide	ultrapure water (pH 9.2; 25 °C)	100% (5 min)
89	halogenated organic	50 µM MCAA	homogeneous	LP-Hg 10 W	1.0 mM sulfite (UPW); 2.0 mM sulfite (river)	ultrapure water; Yangtze River, China (pH 9.2; 25 °C)	100% (15 min in ultrapure water; 75 min in river water)
106	halogenated organic	300 µM Diclofenac	homogeneous	LP-Hg (n.r. W)	8.0 mM sulfite	ultrapure water (pH 9.2; room temp)	98% (30 min)
107	halogenated organic	600 µM 2,4-dichlorophenol	homogeneous	LP-Hg (n.r. W)	8.0 mM sulfite	ultrapure water (pH 10; n.r °C)	99.45% (40 min)
39	halogenated organic	0.6 mg L^{-1} vinyl chloride	homogeneous	LP-Hg 36 W	20 mg L^{-1} sodium dithionite; 12.5 mg L^{-1} sodium sulfite; 8.4 mg L^{-1} sodium hydrosulfide; 49 mg L^{-1} ferrous sulfate	ultrapure water (pH 3,7,10; n.r. °C)	varies
108	halogenated organic	1 mg L^{-1} vinyl chloride	homogeneous	LP-Hg 36 W	0.16 mM sulfite	ultrapure water (pH 9; 34 °C)	100% (90 min)
109	halogenated organic	10 mg L^{-1} difluoroacetic acid	homogeneous	LP-Hg 8 W	1.0 mg L^{-1} iodide	ultrapure water (pH 9; 20 °C)	n.r.
110	halogenated organic	10 mg L^{-1} trichloroethylene	homogeneous	LP-Hg 36 W	10.0 mM sulfite	ultrapure water (pH 10; 20 °C)	100% (60 min)
46	halogenated organic	250 mg L^{-1} 2, 4, 6-trichlorophenol	homogeneous	LP-Hg (n.r. W)	6.2 mM sulfite	ultrapure water (pH 7; 20 °C)	100% (80 min)
111	halogenated organic	30 mg L^{-1} Acid Yellow 17	homogeneous	LP-Hg 6 W	1.5 mM dithionite	ultrapure water (pH 9; n.r. °C)	90% (5 min)
112	halogenated organic	5 mg L^{-1} tetrachloromethane	homogeneous	LP-Hg 14 W	10.0 mM sulfite	ultrapure water (pH 9; n.r. °C)	100% (5 min)
113	halogenated organic	50 mg L^{-1} pentachlorophenol	homogeneous	LP-Hg 16 W	100 mg L^{-1} dithionite; 100 mg L^{-1} phenol	ultrapure water (pH 7; n.r. °C)	96% (180 min)
114	halogenated organic	2 µM iopamidol	homogeneous	LP-Hg 10 W	0.5 mM sulfite	ultrapure water (pH 7; 20 °C)	80% (30 min)
115	organic	21.16 µM carbamazepine	homogeneous	LP-Hg (n.r. W)	1.6 mM sulfite	ultrapure water (pH 8.4; room temp)	100% (10 min)
116	organic	30 µM dinitrotoluene	homogeneous	LP-Hg 10 W	0.05 mM toluene	ultrapure water (pH 7.5; 25 °C)	100% (20 min)
20	oxidized transition metal	5 mg L^{-1} Cr(VI)	homogeneous	MP-Hg 300 W	5.0 mM sulfite	ultrapure water (pH 5–10.5; 20 °C)	100% (20 min with pH 5)
21	oxidized nonmetal	10 mg L^{-1} Se(VI)	heterogeneous (Fe(III) co-agulation)	MP-Hg 300 W	5.0 mM sulfite	ultrapure water (pH 9.2; 20 °C) (HA DOM spike)	99% (20 min without HA); 72% (20 min with HA)

Table 3. continued

ref	compound class	[compound]$_0$ (μM)	heterogeneous or homogeneous system	UV lamp	UV sensitizer	water characteristics	parent compound degradation % (time)
19	oxyanion	100 μM bromate	heterogeneous (Fe(II)–Ti(IV)) LDH Nanoparticles	LP-Hg 15 W	0.5 g L^{-1} Fe(II)–Ti(IV)	tap water (pH 7; 25 °C)	90% (1 h)
16	oxyanion	4 μM bromate	homogeneous	LP-Hg 8 W; MP-Hg 150 W	varying sulfite	ultrapure water (pH varies; 26 °C)	100% (varies)
14	oxyanion	6.6 μM bromate	heterogeneous (superparamagnetic BiOCl)	LP-Hg 10 W	4.0 mM formate	ultrapure water (pH 7; 25 °C)	79% (15 min)
117	oxyanion	10 μM bromate	homogeneous	LP-Hg 10 W	1.0 mM sulfite/0.1 mM iodide	ultrapure water (pH 9.2; 20 °C)	100% (5 min)
15	oxyanion	39 μM bromate	homogeneous	LP-Hg 15 W	0.78 mM sulfite	ultrapure water (pH 9.8; n.r. °C)	86% (4 h)
18	oxyanion	100 μM bromate	homogeneous	LP-Hg 15 W; MP-Hg 100 W	2.0 mM sulfur(IV)	ultrapure water; tap water (pH 9; 25 °C)	82% (20 min in tap water); 99% (20 in ultrapure water)
6	oxyanion	2.75 μM bromate	homogeneous	LP-Hg 36 W	25.6 mg L^{-1} sulfite	ultrapure water (pH 7, n.r. °C)	100% (125 min in LP)
118	oxyanion	100 μM bromate	homogeneous	LP-Hg 10 W	1.0 mM sulfite	ultrapure water (pH 7; 23 °C) (HA DOM spike)	20% (40 min)
119	oxyanion	160 μM nitrate	homogeneous	LP-Hg 36 W	8.4 mM sulfite	ultrapure water (pH 9; 27 °C)	100% (20 min)
113	oxyanion	50 mg L^{-1} nitrate	homogeneous	LP-Hg 16 W	100 mg L^{-1} dithionite; 100 mg L^{-1} phenol	ultrapure water (pH 7; n.r. °C)	94% (180 min)
11	oxyanion	50 mg L^{-1} nitrate	homogeneous	LP-Hg (n.r. W) (254 and 185 nm)	none	ultrapure water (pH 6; 25 °C)	99% (80 min)
120	oxyanion	2 μM nitrate	homogeneous	LP-Hg 9 W	60 mM sulfite	ultrapure water (pH 9.2; 25 °C)	100% (90 min)
12	oxyanion	100 μM perchlorate	homogeneous	LP-Hg 36 W	11.0 mM sulfite	ultrapure water (pH 11; n.r. °C) (SRHA DOM spike)	10% (25 h, 50 mg/L SRHA) 80% (25 h, 0 mg/L SRHA)
13	oxyanion	100 μM perchlorate	homogeneous	LP-Hg 36 W	3.76 mM sulfite	ultrapure water (pH 11; 30 °C)	20% (10 h)
64	PFAS	10 μM PFOS	homogeneous	LP-Hg 14 W	2.0 mM nitrilotriacetic acid	ultrapure water (pH 10; 30 °C)	85.4% (10 h)
121	PFAS	20 μM PFOA	homogeneous	LP-Hg 15 W	0.6 mM iodide	ultrapure water (pH 9.2; 20, 25, 40 °C)	98% (6 h), 99% (6 h), 100% (6 h)
28	PFAS	24 μM PFOA	heterogeneous (self-assembled micelle with cationic surfactant)	HP-Hg 500 W	1.0 mM indoleacetic acid	ultrapure water (pH 4–8; 25 °C)	90% (2.5 h)
22	PFAS	25 μM PFOA	homogeneous	LP-Hg 15 W	0.3 mM iodide	ultrapure water (pH 9; room temp)	95% (6 h)
122	PFAS	25 μM PFOA	homogeneous	LP-Hg 15 W	0.25 mM iodide	ultrapure water (pH 5, 7, 10; n.r. °C)	9.1% (2 h), 74.6% (2 h), 97.9% (2 h)
123	PFAS	25 μM PFCA	homogeneous	LP-Hg 18 W	10.0 mM sulfite	ultrapure water (pH 12; 20 °C)	varies
33	PFAS	25 μM PFCAs, PFSAs, fluorotelomers	homogeneous	LP- Hg 18 W	10.0 mM sulfite	ultrapure water (pH 12; 20 °C)	varies (4 h)
78	PFAS	32 μM PFOS	homogeneous	HP-Hg 250 W	10.0 mM sulfite	ultrapure water (pH 9.2; 25 °C)	98% (0.5 h)

Table 3. continued

ref	compound class	[compound]$_0$ (μM)	heterogeneous or homogeneous system	UV lamp	UV sensitizer	water characteristics	parent compound degradation % (time)
124	PFAS	37.2 μM PFOS	homogeneous	MP-Hg 500 W	none	ultrapure water (pH 7.4; 90 °C)	90% (11 days)
77	PFAS	38.7 μM PFOA	homogeneous	HP-Hg 250 W	10.0 mM sulfite	ultrapure water (pH 9.2; 25 °C)	100% (10 min)
25	PFAS	10 mg L^{-1} PFOA; 10 mg L^{-1} PFOS	heterogeneous (organo-montmorillonite)	LP-Hg 36 W	1.0 mM 3-indoleacetic acid	ultrapure water (pH 3–11; 25 °C)	100% (5 h)
1	PFAS	10 mg L^{-1} PFOS, PFOA, PFHS, PFBS, PFHA, PFBA	homogeneous	LP-Hg 8 W	10.0 mM iodide	ultrapure water (pH 6–8; n.r. °C)	5–30% (150 min)
34	PFAS	Varying AFFF (15 PFAS)	homogeneous	LP-Hg 18 W	10.0 mM sulfite	ultrapure water (pH 9.5; 20 °C)	varies
23	PFAS	PFOA	homogeneous	LP-Hg 10 W	10.0 mM sulfite	ultrapure water (pH 10.3; 25 °C)	100% (1 h)
30	PFAS	25 μM PFCAs	homogeneous	LP-Hg 18 W	10.0 mM sulfite	ultrapure water (pH 9.5; 20 °C)	100% (8–12 h)
31	PFAS	25 μM PFECAs	homogeneous	LP-Hg 18 W	10.0 mM sulfite	ultrapure water (pH 9.5; 20 °C)	varies
125	PFAS	30 μM PFOA	homogeneous	LP-Hg 14 W	0.3 mM iodide	ultrapure water (pH 10; 25 °C) (HA DOM spike)	67.5% (1.5 h)
58	PFAS	30 μM PFOS	homogeneous	LP-Hg 14 W	0.3 mM iodide	ultrapure water (pH 10; 25 °C) (HA DOM spike)	86% (1.5 h)
24	PFAS	37.2 μM PFOS	homogeneous	LP-Hg 10 W (254 and 185 nm)	20 mM sulfite	ultrapure water (pH 10; 25 °C) (HA DOM spike)	97.3% (4 h without HA); 85% (4 h with HA)
27	PFAS	24 μM PFOA	heterogeneous (self-assembled micelle with cationic surfactant)	LP-Hg 36 W	1.0 mM indole-acetic acid	ultrapure water (pH 6; 25 °C) (SRHA and SRFA DOM spike)	100% (6 h)
29	PFAS	24 μM PFOA	homogeneous	LP-Hg 36 W	1.0 mM indole-3-acetic acid; 1.0 mM indole-1-acetic acid; 1.0 mM indole-3-carboxylic acid; 1.0 mM indole; 1.0 mM skatole; 1.0 mM donaxine	ultrapure water (pH 6; 25 °C)	35.7% (8 h); 31.4% (8 h); 24.4% (8 h); 100% (8 h); 100% (8 h); 100% (8 h)
26	PFAS	24.1 μM PFOA	heterogeneous (organo-montmorillonite)	LP-Hg 36 W	1.0 mM 3-indole-acetic acid; 1.0 mM indole; 1.0 mM 3-indole-carboxylic acid; 1.0 mM 3-methylindole	ultrapure water (pH 6; 25 °C) (SRHA DOM spike)	100% (5 or 8 h with DOM spike; 3-indole-acetic acid)

^{a}n.r. is used to indicate if information was not reported by authors. UV sensitizer specified as "none" refers to vacuum UV studies.

They may also fail to adequately describe experimental data in complex reaction systems where it is simply not possible to know all the reactions.[97] For these reasons, computer kinetics models may be most beneficial for estimating unknown parameters for a specific UV-ARP and understanding the impact of design and process variables on treatment performance.

2.4.3. The Role of Dissolved Organic Matter. While some prior research has evaluated the impact of dissolved organic matter (DOM) on target contaminant transformation in UV-ARP, more work is needed to fully understand the role of DOM in e_{aq}^--based treatment systems. While it is expected that DOM is an important e_{aq}^- scavenger, specific bimolecular rate constants are not yet established. Dissolved oxygen, nitrate, and nitrite, which all exhibit high reactivity with e_{aq}^-, will likely dominate the e_{aq}^- scavenging at low e_{aq}^- exposures (Figures 5 and 6). However, given the variety of structural moieties present, DOM may exert a significant e_{aq}^- scavenging capacity long into the UV-ARP process. In addition, the impact of e_{aq}^- exposure on DOM light absorption in UV-ARP systems needs to be further evaluated, although prior studies indicate that various reduction methods (borohydride,[98] electrochemical,[99] and UV/sulfite[12]) decreases DOM absorbance. Changes in DOM absorbance at the actininic wavelength(s) will impact the rate of light absorption by the sensitizer and therefore the rate of e_{aq}^- formation in the system.

3. UV-ARP SUBSTRATE SCOPE

Previous research has evaluated the suitability of UV-ARP for degradation of both inorganic and organic contaminants. Target contaminants that have been considered for UV-ARP treatment typically have a high oxidation state central atom (e.g., N in NO_3^-) or one or more carbon—halogen bonds as part of their structure. Indeed, previous computational studies showed that bimolecular e_{aq}^- reaction rate constants were inversely proportional to the energy of the lowest unoccupied molecular orbital (E_{LUMO}) for a large set (>100) of substituted aliphatic compounds.[100,101]

As part of this Review, we have compiled literature data from UV-ARP treatment studies of important inorganic and organic contaminants. Table 3 presents a summary of these UV-ARP studies separated by compound class, which includes details like lamp power and type (low-, medium-, or high-pressure Hg), e_{aq}^- sensitizer, solution conditions, and degradation rates (final % degraded and reaction time). A searchable copy of Table 3 including additional details (e.g., average UV fluence rate and sparging conditions) is included in the Supporting Information. The sections below highlight key results from this analysis for oxyanions, halogenated organics, and PFAS.

3.1. Oxyanions

UV-ARP technologies have been studied for the degradation of oxyanions such as NO_3^-, NO_2^-, ClO_4^-, and BrO_3^-,[6,10−19] which contain a highly oxidized central atom. The reaction mechanism involves e_{aq}^- addition to the central atom and loss of $O^{\bullet-}$ (the conjugate base of $^\bullet OH$). The conversion of bromate to bromite is shown in Figure 9 as an example.

Many oxyanions have been shown to be degraded quickly by e_{aq}^- generated in UV-ARP (e.g., NO_3^-, NO_2^-, BrO_3^-),[16,18,120] while ClO_4^- reacts more slowly.[12,13,126] Conversion of oxyanions to benign end products requires further reduction of intermediate products.[119,127] For example, NO_3^- reacts with e_{aq}^- to produce NO_2^- which is reduced further through additional reactions with e_{aq}^- to eventually produce N_2.
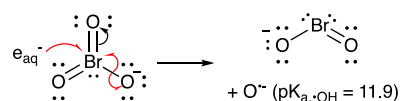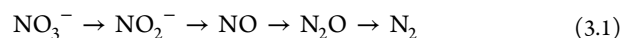
Figure 9. Reaction of e_{aq}^- with bromate (BrO_3^-) to form bromite (BrO_2^-) and $O^{\bullet-}$. Although shown as a concerted process, a one-electron adduct (BrO_3^{2-}) may be formed prior to Br—O bond homolysis.

$$NO_3^- \rightarrow NO_2^- \rightarrow NO \rightarrow N_2O \rightarrow N_2 \qquad (3.1)$$

Given sufficient e_{aq}^- exposure, it may be possible to quantitatively produce the free halides of halogen-containing oxyanions.[13,15,18] For example, bromite is completely degraded during UV/sulfite treatment and yields bromide as the only product. Conversely, even at higher $[SO_3^{2-}]$, higher light intensity, and longer reaction times, ClO_4^- treatment by UV/sulfite treatment has not achieved 100% abatement. However, Vellanki et al. showed that perchlorate degradation during UV/sulfite treatment was significantly enhanced at pH 12 (∼75% abatement) relative to pH 9 (∼25% abatement[7]). In the case of ClO_4^-, Cl^- and ClO_3^- were the only transformation products observed. This suggests that the rate limiting step is either e_{aq}^- reduction of ClO_4^- or ClO_3^-, which is consistent with very slow e_{aq}^- bimolecular rate constants for these species ($k < 10^6 M^{-1} s^{-1}$) and the much faster values for ClO_2^- and ClO^- (>$10^9 M^{-1} s^{-1}$). Consequently, entries in Table 3 reveal huge differences in UV-ARP treatment effectiveness for BrO_3^- and ClO_4^-, consistent with the fact that ClO_4^- is frequently employed as an "inert" electrolyte.

The reactivity of oxyanions with e_{aq}^- depends on several key factors. The affinity for oxyanion reduction by e_{aq}^- is based primarily on the availability of an electron orbital offered by the central atom, not the compound's one-electron redox potential.[127] For example, NO_2^- reacts with e_{aq}^- more slowly ($k = 3.5 \times 10^9 M^{-1} s^{-1}$)[128] than NO_3^- ($k = 9.7 \times 10^9 M^{-1} s^{-1}$),[8] which is opposite of what one would expect from the NO_2^-/NO redox couple[129] ($E° = 0.46$ V) vs (NO_3^-/NO_2^- of 0.10 V[130]). The oxyanion's molecular geometry and charge of the central atom can further impact their reduction by e_{aq}^-. For example, NO_3^- is more reactive with e_{aq}^- than ClO_4^- ($k < 1.6 \times 10^6 M^{-1} s^{-1}$).[129] While the Cl atom in ClO_4^- is at a higher oxidation state (+7) than N in NO_3^- (+5), the slower reactivity of e_{aq}^- may be attributed to the planar structure of NO_3^-, facilitating e_{aq}^- interaction versus the inhibiting tetrahedral structure of ClO_4^-.[127]

Additional radical species can also contribute to oxyanion degradation occurring in UV-ARP. For example, Vellanki and Batchelor proposed that $SO_3^{\bullet-}$ is the main reactive species responsible for the reduction of ClO_4^- in the UV/sulfite system.[13] In this case, it was proposed that $SO_3^{\bullet-}$ abstracts an oxygen atom from ClO_4^- to form the sulfate radical and chlorate.[13] Similarly, the carbon dioxide radical anion ($CO_2^{\bullet-}$) was proposed to be the main reducing agent responsible for BrO_3^- and NO_3^- reduction in the UV/formate system.[10,14] Moussavi and Shekoohiyan discovered that hydrogen atoms ($H^\bullet$) are responsible for a small percentage of NO_3^- reduction under VUV irradiation (185 nm radiation wavelength).[11] In addition, $H^\bullet$ are the main reactive species responsible for BrO_3^- degradation under acidic conditions[6,18] due to increased formation of $H^\bullet$ from the reaction of H^+ and e_{aq}^- (Table 1).

3.1.1. Other Inorganic Species. UV-ARP have also been studied for the removal of oxidized metal ions such as chromium(VI) and nonmetals like selenium(IV).[20,21] The e_{aq}^- reduction lowers the oxidation state of these contaminants,
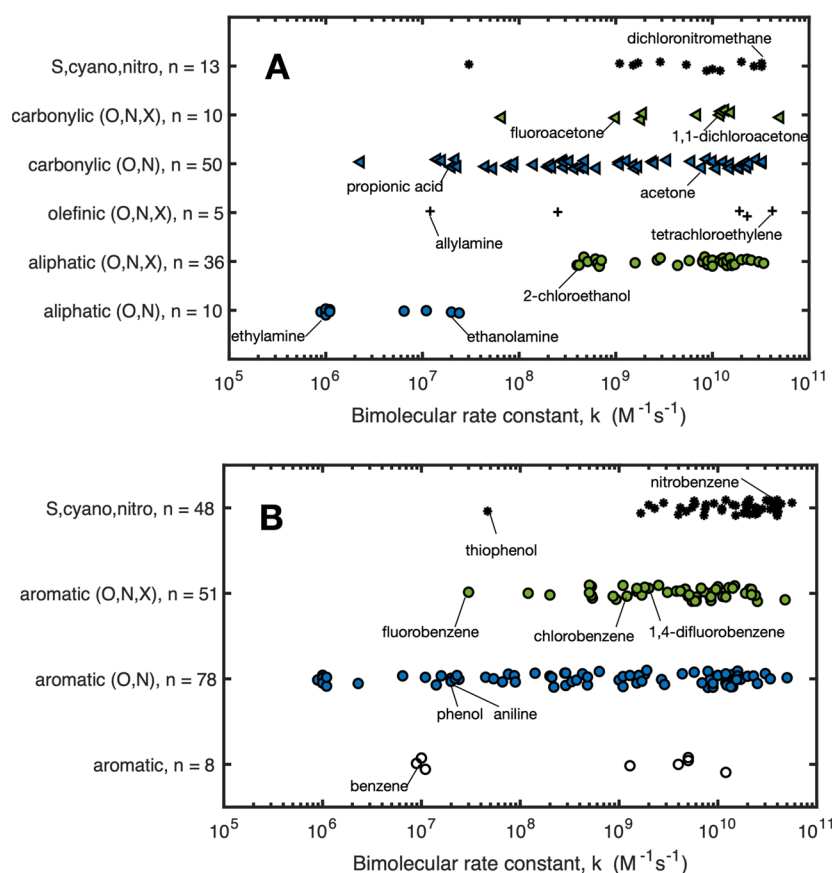
Figure 10. Bimolecular rate constants for reaction of hydrated electron with nonaromatic (A) and aromatic (B) compounds. Rate constants are from Li et al.[100] and are tabulated by compound class in the Supporting Information. Compound classes are differentiated by the presence of O, N, and X = F, Cl, Br, I atoms. The number of compounds in each class is represented by *n*. Selected compounds are shown within each class to compare trends in reactivity.

which decreases their solubility and often induces precipitation. For example, UV/dithionite treatment completely removed selenite through this combined reduction/precipitation process after ~120 min.[21] In the case of chromium, UV/sulfite treatment between pH 5 and 10 effectively reduced Cr(VI) to Cr(III), followed by precipitation of Cr(III) salts.[20] While other approaches can also be used for reductive precipitation of Cr(VI) and Se(IV), reduction by e_{aq}^- occurs readily at neutral and basic pH, while other reductants are limited by the decreased reduction potential of Cr(VI) and Se(IV) with increasing pH.

3.2. Organic Compounds

In addition to inorganic contaminants, a number of studies have evaluated UV-ARP for the degradation of halogenated contaminants. Below, we discuss UV-ARP based treatment for halogenated organic compounds, including chlorinated and brominated contaminants. A separate section is devoted to PFAS given the currently high level of interest in e_{aq}^--based treatment for these compounds. For readers interested in further understanding the reactivity of e_{aq}^- with organic compounds beyond halogenated contaminants, the book chapter by Anbar entitled "The Reactions of Hydrated Electrons with Organic Compounds" provides a thorough discussion of e_{aq}^- reactivity with various organic functional groups.[131]

3.2.1. Halogenated Organic Compounds. The reactivity of organic compounds with e_{aq}^- in terms of bimolecular rate constants has been studied for many decades.[8,131,132]

Bimolecular rate constants for e_{aq}^- with organic compounds vary widely depending on compound class and the presence of halogen atoms (Figure 10). For example, aliphatic compounds bearing only N and O atoms, regardless of the functional group, have substantially lower reactivity than aliphatic compounds also bearing halogen atoms. Halogen atom substitution on carbonylic and aromatic compounds also generally increases their reactivity with e_{aq}^-. An exception is that, for nonaromatic compounds, substituting −H with −F tends to decrease the reactivity with e_{aq}^- (e.g., acetone vs fluoroacetone, Figure 10A). For aromatic compounds, substituting −H with −F slightly increases its reactivity with e_{aq}^- and this is further enhanced when multiple −F are substituted (e.g., benzene, fluorobenzene, 1,4-difluorobenzene, Figure 10B).

3.2.1.1. Haloaliphatic Compounds. In a homologous series of halogenated aliphatic compounds, the reactivity with e_{aq}^- typically follows the trend F ≪ Cl < Br < I.[131] For example, the relative reactivity of fluoroacetate, chloroacetate, bromoacetate, and iodoacetate is 0.002 < 1.0:6.2:12.0 (Figure 11).[8] This trend demonstrates that the C−X bond is more reactive than the
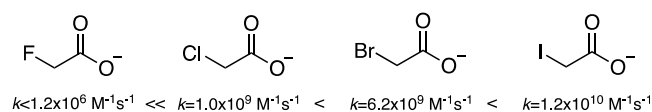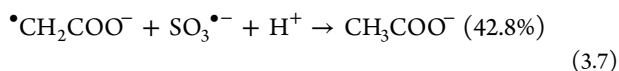

$k<1.2\times10^6$ M^{-1}s^{-1} ≪ $k=1.0\times10^9$ M^{-1}s^{-1} < $k=6.2\times10^9$ M^{-1}s^{-1} < $k=1.2\times10^{10}$ M^{-1}s^{-1}
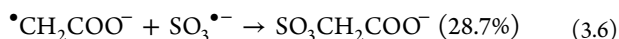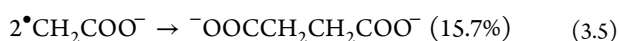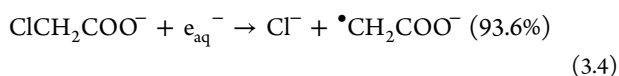
Figure 11. Relative reactivity of monosubstituted haloacetate ions with hydrated electron in terms of their bimolecular reaction rate constant.

carboxyl group.[91] Indeed, acetate's reactivity with e_{aq}^- ($k = 1.1 \times 10^6$ M^{-1} s^{-1}) is comparable to that of fluoroacetate.[8]

Reductive dehalogenation of haloaliphatic compounds is thought to occur via a two-step reaction, in which a reduced intermediate, RX$^{\bullet-}$, is first formed which subsequently undergoes unimolecular dissociation:[131]

$$RX + e_{aq}^- \rightarrow RX^{\bullet-} \quad (3.2)$$

$$RX^{\bullet-} \rightarrow R^\bullet + X^- \quad (3.3)$$

with the products of the second step being a carbon centered radical (R$^\bullet$) and halide (X$^-$). The fate of the carbon centered radical depends on the water matrix composition. Since UV-ARP seek to maintain low [O$_2$], the formation of peroxyl radicals is not expected to be a significant sink of R$^\bullet$. As an example, the following reaction pathway for UV/sulfite transformation of chloroacetate in laboratory grade water has been established (eqs 3.4–3.7[57])

$$ClCH_2COO^- + e_{aq}^- \rightarrow Cl^- + {}^\bullet CH_2COO^- \ (93.6\%) \quad (3.4)$$

$$2 {}^\bullet CH_2COO^- \rightarrow {}^- OOCCH_2CH_2COO^- \ (15.7\%) \quad (3.5)$$

$${}^\bullet CH_2COO^- + SO_3^{\bullet-} \rightarrow SO_3CH_2COO^- \ (28.7\%) \quad (3.6)$$

$${}^\bullet CH_2COO^- + SO_3^{\bullet-} + H^+ \rightarrow CH_3COO^- \ (42.8\%) \quad (3.7)$$

where the percent yields in parentheses are based on the observed rates of product formation relative to the rate of chloroacetate degradation. Chloride is formed at near 100% yield. Several additional carbon-containing products were also observed with varying yields, including succinic acid (formed from coupling of two ${}^\bullet CH_2COO^-$ radicals), sulfoacetic acid (radical coupling of $SO_3^{\bullet-}$ and ${}^\bullet CH_2COO^-$), and acetate (possibly due to reduction of ${}^\bullet CH_2COO^-$ by $SO_3^{\bullet-}$).

For haloaliphatic compounds, UV-ARP studies have largely focused on haloacetic acids and vinyl chloride.[39,57,60,89,102,108] Direct photolysis is typically an unimportant pathway for haloaliphatic compounds. Liu et al. studied the dechlorination of trichloroacetic acid using UV/titanium dioxide with formate and suggested that both $CO_2^{\bullet-}$ and e_{aq}^- reactions were occurring.[102] Other dechlorinated products such as di- and monochloroacetic acid are formed during the reaction between trichloroacetic acid and e_{aq}^-. Vinyl chloride can be degraded by UV-ARP through both direct photolysis (due to its unsaturated carbon–carbon bond) and reaction with radical species.[39,108] In the UV/sulfite ARP, Liu et al. found that the rate of vinyl chloride dechlorination was inversely proportional to solution pH.[108] At pH 9, UV/sulfite treatment resulted in ~88% dechlorination. Since e_{aq}^- is the main product of sulfite photolysis at this pH (see Section 2.3), this result suggests that at pH 9 the major mechanism of vinyl chloride degradation is reductive dechlorination induced by e_{aq}^-. Conversely, at pH 7, only ~18% of the total [Cl$^-$] possible was produced. Liu et al. proposed that the low dechlorination of vinyl chloride at pH 7 was due to the reaction of $SO_3^{\bullet-}$ or H$^\bullet$ (the products HSO$_3^-$ photolysis) with the C=C bond to produce chloroethane (identified by GC-MS).[108]

3.2.1.2. Haloaromatic Compounds. Haloaromatic compounds exhibit a similar trend in their reactivity with e_{aq}^- as haloaliphatic compounds, but the fluorinated analogues tend to be more reactive than their aliphatic counterparts. This is demonstrated in Figure 12, which shows the bimolecular
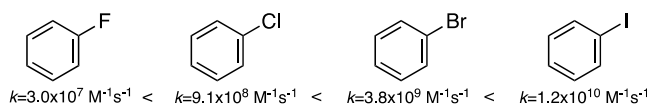

k=3.0x10^7 M^{-1}s^{-1} < k=9.1x10^8 M^{-1}s^{-1} < k=3.8x10^9 M^{-1}s^{-1} < k=1.2x10^{10} M^{-1}s^{-1}

Figure 12. Relative reactivity of aryl halides with hydrated electron in terms of their bimolecular reaction rate constant.

reaction rate constants for the aryl halide series. Iodobenzene is approximately 3 orders of magnitude more reactive than the fluorobenzene (like haloacetic acids in Figure 11). However, the difference in reactivity between fluorobenzene and chlorobenzene (factor of ~30) is less than for the haloacetate ions (factor of ~1000).

Halogenated phenols such as 4-bromophenol, 2,4-dichlorophenol, 2,4,6-trichlorophenol, and pentafluorophenol can also be degraded by UV-ARP.[45,46,104,107,133,134] Direct photolysis contributes to the transformation of these compounds in UV-ARP systems.[45,46] The e_{aq}^--induced reaction pathways for halophenols have been studied in detail,[135,136] with halides being produced quantitatively upon reductive electron capture by the aromatic ring.[136] Phenoxyl radicals are believed to be the initial nonhalogenated products following halide loss.[135]

From a treatment perspective, Xie et al. found that the UV/sulfite ARP completely debrominated 4-bromophenol within 10 min,[45] and quenching experiments with nitrate and nitrite suggested that this degradation was induced by the reaction with e_{aq}^-. Similarly, Yu et al. observed that 2,4-dichlorophenol could be degraded with the UV/sulfite ARP, demonstrating that the reaction with e_{aq}^- is the main reactive species responsible for its degradation.[107] For fluorinated phenols, Shoute et al. reported that the rate constant between e_{aq}^- and pentafluorophenol was fast (2.4×10^{10} M^{-1} s^{-1}) and that a fluoride ion was eliminated to yield a tetrafluorophenoxyl radical.[134] This study only evaluated the bimolecular rate constant for e_{aq}^- reaction with pentafluorophenol and not its degradation or defluorination percentage under steady-state UV-ARP treatment.

3.2.2. Halide Yields. While bimolecular rate constants provide some important information regarding the e_{aq}^--based transformation of contaminants in water, the halide ion yield (i.e., mol of halide formed per mol of e_{aq}^--substrate reaction) is also an important factor, as this parameter defines the overall reaction efficiency. The rate of formation of the reduction product (e.g., halide) is given by[137]

$$R_f^{X^-} = R_f^{e_{aq}^-} \gamma_{e_{aq}^-, X^-} \frac{k_{TC,e_{aq}^-}^t}{k_{TC,e_{aq}^-}^q} \quad (3.8)$$

where $R_f^{X^-}$ is the rate of halide ion formation (M s^{-1}), $R_f^{e_{aq}^-}$ is the rate of e_{aq}^- formation (M s^{-1}), $\gamma_{e_{aq}^-, X^-}$ is the halide ion yield, and $k_{TC,e_{aq}^-}^t$ and $k_{TC,e_{aq}^-}^q$ are the bimolecular rate constants (M^{-1} s^{-1}) for transformation of e_{aq}^- by the target contaminant and quenching of the target contaminant by e_{aq}^-, respectively. e_{aq}^- bimolecular rate constants are typically measured by directly observing the decay kinetics of the e_{aq}^- transient in the near-infrared, which yields the quenching rate constant $k_{TC,e_{aq}^-}^q$. For radical reactions, it is typically assumed that $k_{TC,e_{aq}^-}^t$ is equivalent to $k_{TC,e_{aq}^-}^q$.[137]

$\gamma_{e_{aq}^-, X^-}$ values are not readily available for most of the substrates (organic or inorganic) for which UV-ARP are considered a possible treatment technology. However, some halide ion yields are available from the radiation chemistry literature (Figure
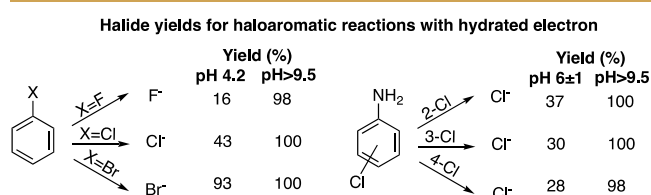
Halide yields for haloaromatic reactions with hydrated electron

Figure 13. Halide ion yields for aryl halide reactions with hydrated electron.[138] Yields are calculated by $G_{X^-}/G_{e_{aq}^-}$ where G_{X^-} is μmol X^-/Gy radiation and $G_{e_{aq}^-}$ is the e_{aq}^- yield from water radiolysis (0.27 μmol/Gy[8]).

13).[138] For benzyl halides, $\gamma_{e_{aq}^-,X^-}$ depends strongly on the halogen substituent and solution pH. At acidic pH (4.2), there is a clear trend of decreasing halide ion yield with increasing electronegativity of the halogen substituent. This trend largely vanishes at basic pH, with fluoro-, chloro-, and bromobenzene having near 100% halide ion yields.

Halide ion yields may also depend on the location of the halogen with respect to other substituents on an aromatic ring (Figure 13). For example, the chloride yield from the reaction of e_{aq}^- with chloroaniline isomers decreases with an increasing number of sigma bonds between the amino and chloro substituents at circumneutral pH. However, at basic pH, $\gamma_{e_{aq}^-,X^-}$ are ~100% for all isomers.

It is also possible to evaluate $\gamma_{e_{aq}^-,X^-}$ in steady-state photochemical experiments by measuring $R_f^{X^-}$ and $R_f^{e_{aq}^-}$. For example, the yield of chloride from reaction with e_{aq}^- is ~0.94 based on the rates of chloroacetate degradation (3.76 $\pm$ 0.07 μM/min) and chloride formation (3.52 $\pm$ 0.01 μM/min) in the UV/sulfite process (see eq 3.4).[57] The experimental conditions (110 μM chloroacetate, 1 mM sulfite, lab grade water) at which these rates were measured are such that most e_{aq}^- should be scavenged by chloroacetate ($k'_{S,t=0} = 110\,000$ s^{-1}). Thus, for $\gamma_{e_{aq}^-,Cl^-} \approx 1$, the initial rate of chloroacetate degradation should be equal to $R_f^{e_{aq}^-}$, as observed.

3.2.3. Per- and Polyfluorinated Alkyl Substances.

Perfluoroalkyl substances are "aliphatic substances for which *all* of the H atoms attached to C atoms in the nonfluorinated substance from which they are notionally derived have been replaced by F atoms, except those H atoms whose substitution would modify the nature of any functional groups present".[139] Polyfluoroalkyl substances are "aliphatic substances for which all H atoms attached to at least one (but not all) C atoms have been replaced by F atoms, in such a manner that they contain the perfluoroalkyl moiety C_nF_{2n+1}".[139] These per- and polyfluoroalkyl substances (PFAS) are characterized by extremely strong C—F bonds, which, combined with their properties as surfactant molecules, makes them extremely difficult to remove from, or degrade in, water.[140]

UV-ARP have increasingly been proposed as a promising technology for e_{aq}^--based transformation of PFAS, although it is interesting to note that Anbar originally described fluorinated aliphatics as "unreactive" toward e_{aq}^- due to fluorine's high electronegativity.[131] Previous reports have demonstrated that it is possible to achieve near 100% reductive defluorination (production of nontoxic fluoride) of some PFAS through UV-

ARP.[22,27,30,33] Although studies of PFOA and PFOS are more common, UV-ARP technology has now been evaluated for many PFAS subclasses, including short- and long-chain perfluoroalkanesulfonates (PFSA),[1,33] perfluoroalkylcarboxylic acids (PFCA),[30,31] perfluoroethercarboxylic acids (PFECA),[31] and fluorotelomer sulfonates and carboxylic acids (Figure 14).[33]
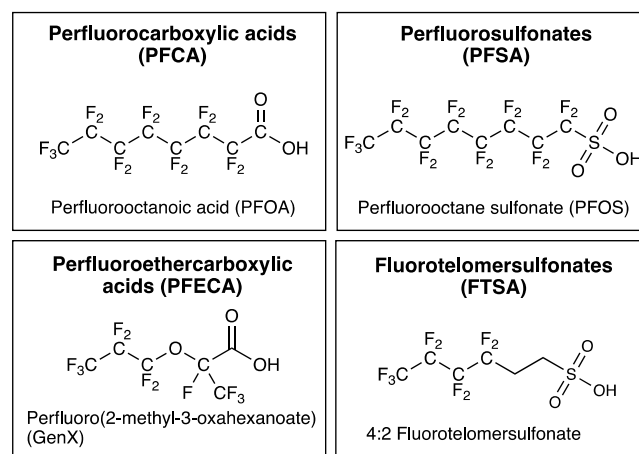

Figure 14. PFAS subclasses referred to frequently in this review, including their acronym and a representative structure.

Additionally, Tenorio et al. investigated UV/sulfite treatment of aqueous film-foaming foam (AFFF), which contains thousands of PFAS, diluted in sodium carbonate buffer at a ratio of 1:60 000.[34] They observed that pseudo-first-order rate constants for degradation of specific PFAS in diluted AFFF were nearly identical to single-compound mixtures in the same sodium bicarbonate buffer system, suggesting that scavenging of e_{aq}^- by AFFF components did not significantly impact $[e_{aq}^-]$.[34]

In one of the earliest UV-ARP PFAS studies, Park et al. investigated the reductive defluorination of perfluorocarboxylic acids and perfluorosulfonates in the UV/iodide system.[1] They found that the headgroup (e.g., $-SO_3^-$ vs COO^-) and $-(CF_2)_n-$ chain length influenced the reductive defluorination kinetics. Specifically, the degradation rate of perfluorosulfonates increased with increasing chain length whereas perfluorocarboxylic acid chain length had little impact on the observed kinetics. Interestingly, Park et al. observed that UV/iodide degradation of PFOS occurred faster than that of PFOA, but several later studies employing UV/sulfite demonstrate an opposite trend in reactivity.[30,34] This result from Park et al. is probably the result their PFAS/KI solutions being at different initial pHs, where the initial pH of PFOS solution was ~7 while for PFOA it was ~4.5. Therefore, quenching of e_{aq}^- by H$^+$ in PFOA solution (pH 4.5, see Table 1) is a likely explanation of its slower transformation than PFOS. Conversely, UV/sulfite studies buffer solution at pH > 9 to maintain SO_3^{2-} as the major S(IV) species,[23,34] which also minimizes e_{aq}^- quenching by H$^+$.

3.2.3.1. PFAS Transformation Mechanisms. The mechanistic understanding of PFAS reductive defluorination has improved in the past few years. In their investigations of UV/sulfite treatment of PFAS sub classes,[30,31,33] Bentel et al. proposed that reductive defluorination can proceed by one of two main mechanisms, as summarized in Figure 15.

The first pathway is H/F atom exchange, in which a $-CF_2-$ group is transformed to a $-CH_2-$ group. This reaction takes two e_{aq}^- and two H$^+$ per H/F exchange. For perfluorocarboxylic acids (like PFOA), H/F exchange is thought to occur preferentially at
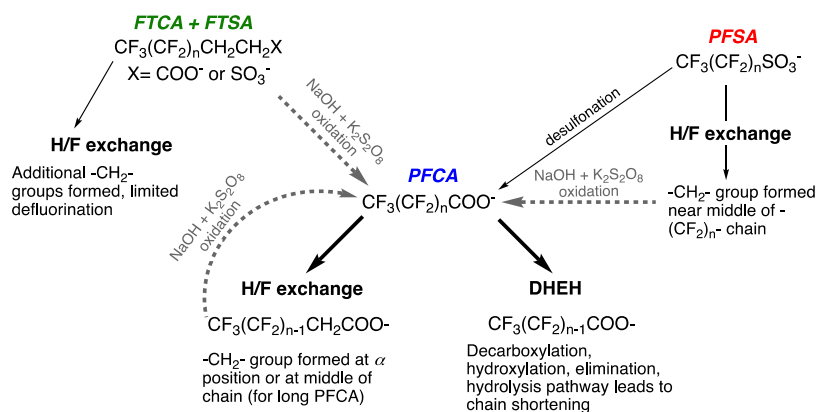
Figure 15. Proposed reaction pathways for the transformation of perfluorocarboxylic acids (PFCA), perfluorosulfonates (PFSA), and fluorotelomercarboxylic acids or fluorotelomer sulfonates (FTCA + FTSA) by hydrated electron (solid, black lines) and hydroxyl radical reactions (dashed, gray lines). Based on work of Bentel et al.[2,30,79] and Liu, Bentel et al.[33]
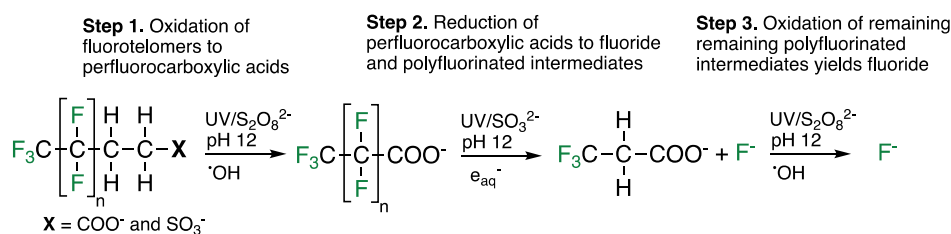

Figure 16. Reaction scheme for the oxidation−reduction−oxidation treatment scheme developed by Liu, Bentel et al. for the near complete defluorination of fluorotelomer carboxylates and sulfonates.[33]

the carbon atom adjacent to the carboxylate headgroup. For perfluorosulfonates (like PFOS), the H/F exchange is thought to occur toward the middle of the chain. This H/F exchange mechanism is supported by the formation of polyfluorinated intermediates identified through nontarget analysis during UV/sulfite treatment of PFAS.[30] Computational chemistry results are also supportive of this mechanism. For example, based on spin density isosurfaces, Van Hoomissen and Vyas showed that an excess electron added to PFOA is localized around the carboxylate headgroup whereas for PFOS$^{\bullet 2-}$ the extra electron is distributed throughout the fluoroalkyl chain in a fashion similar to perfluorooctane.[141] The location of e_{aq}^{-} reaction during H/F exchange also relates to the positive correlation between chain length and perfluorosulfonate reactivity with e_{aq}^{-} reported in several studies.[1,30,34] For example, aqueous vertical attachment energies correlated positively to the chain length of perfluorosulfonates but not perfluorocarboxylic acids.[141] Additionally, Bentel et al. demonstrated that perfluorosulfonate C−F bonds with the lowest bond dissociation energy tended to be toward the middle of the perfluoro chain whereas the lowest energy C−F bonds in perfluorocarboxylic acids tended to be adjacent to the carboxylate group.[30]

The product of H/F exchange is a polyfluorinated substance and UV/sulfite studies show that polyfluorinated substances like fluorotelomercarbxylic acids (FTCA) are less reactive toward e_{aq}^{-}.[30,34] Thus, reaction via H/F exchange limits the complete defluorination of PFAS. To address this problem, Liu, Bentel et al. recently demonstrated that greater reductive defluorination of PFAS could be achieved by performing both reductive and oxidative treatments in sequence.[33] These reaction pathways are highlighted in the context of UV-ARP treatment in Figure 15 with additional details relevant to the study of Liu, Bentel et al.[33] shown in Figure 16. In brief, polyfluorinated compounds formed

during pH 12 UV/sulfite treatment of perfluorocarboxylic acids or perfluoroalkanesulfonates (H/F exchange) could be further defluorinated by subsequent •OH oxidation via high temperature NaOH + $K_2S_2O_8$. When employing fluorotelomer sulfonates and carboxylates as the starting contaminant, a sequence of oxidation−reduction−oxidation was able to achieve near 100% defluorination for most chain lengths (Figure 16).

The second reaction pathway is decarboxylation-hydroxylation-elimination-hydrolysis (DHEH) and is thought to occur only for perfluorocarboxylic acids. The DHEH mechanism is proposed to shorten the perfluoroalkyl chain by one −CF_2− group in each step. The decarboxylation leads to a perfluorinated alcohol, which is susceptible to HF elimination. The DHEH mechanism results in chain shortening and so-called "deeper" levels of defluorination than H/F exchange.[30] Note that perfluorosulfonates do not undergo DHEH directly but could do so after desulfonation, which has been proposed to explain the formation of PFOA and other perfluorocarboxylic acids during UV/sulfite treatment of PFOS.[30] The mechanism is supported in part by the significantly faster kinetics and greater defluorination percentage of perfluorocarboxylic acid abatement during UV/sulfite treatment at pH 12 relative to pH 9.5.[123] Perfluoroether carboxylic acids (e.g., GenX) were proposed to undergo a similar reduction pathway, with cleavage of the C−O ether bond helping to enhance formation of the unstable perfluoroalcohol.[31]

Collectively, the reductive defluorination mechanisms discussed above suggest that the abatement of parent PFAS and ultimate fluoride production is determined by more than just the availability of e_{aq}^{-}. The reactivity of PFAS transformation products with e_{aq}^{-} appears to be an important controlling factor. Thus, biasing solution conditions to favor the DHEH reaction pathway (e.g., high pH) could enhance reductive defluorination.

3.2.3.2. Optimizing PFAS Treatment by UV-ARP. Multiple studies have investigated the conditions needed to optimize PFAS treatment by increasing its e_{aq}^- exposure.[1,2,22−25,58,64,121,122,124,125] For example, UV irradiation of sulfite, iodide, nitrilotriacetic acid, and several indoleacetic acid derivatives have all been shown to degrade PFOA or PFOS through reductive defluorination by e_{aq}^-, all with varying kinetic rates.[22,23,25,64] However, no single study has compared all these e_{aq}^- sensitizers under equivalent photochemical conditions. Sun et al. demonstrated that the UV/nitrilotriacetic ARP led to faster defluorination of PFOS than UV/sulfite at an equivalent concentration (2 mM), but it is important to note that nitrilotriacetic acid has a higher molar absorption coefficient (ε_{254} = 26.3 M^{-1} cm^{-1} at pH 10[64]) at the actinic wavelength (254 nm) than sulfite ($\varepsilon_{254} \approx 18$ M^{-1} cm^{-1}[57]) (see Table 2). In addition, Yu et al. showed that combining sulfite and iodide into one system yielded faster rates of reductive dechlorination of a monochloroacetate system[60] (this UV/sulfite/iodide system has not yet been applied to PFAS degradation). The UV/indoleacetic acid system is ineffective at degrading PFOA in bulk, aqueous solution (see further below).[25]

Additional treatment conditions studied for PFOA and PFOS degradation includes the initial solution pH, temperature, and the presence of e_{aq}^- scavenging species like O_2, NO_3^-, NO_2^-, and DOM.[1,2,22−24,58,121,122,124,125] Higher temperatures resulted in faster degradation kinetics for PFOA and PFOS, with apparent activation energies of ∼50 and 25 kJ/mol, respectively, in the UV/iodide system.[121,124] Qu et al. demonstrated the major scavenging impact of O_2 on PFOA degradation; when *continuously* sparging solutions with O_2, the percent defluorination decreased from ∼98% (under N_2 saturation) to less than 5% (O_2-saturated solution).[22] However, Bentel et al. showed that initial sparging of reaction solutions with N_2 made no difference in the removal kinetics of PFOA,[30] which could be explained by O_2 removal through reaction with sulfite, either through a thermal[51] or photochemical process[68] at early UV-ARP treatment times (see also Figure 6).

Gu et al. found that PFOS degradation in the UV/sulfite ARP was significantly inhibited by humic acid (≥2.64 mgC/L) and NO_3^- (≥0.5 mM NO_3^-), whereas HCO_3^- had minimal impact at a concentration of 1.0 mM.[24] The decreased reactivity of PFOS in the UV/sulfite system in the presence of humic acid (a surrogate for DOM) could be due to the following three mechanisms: (1) shielding of the e_{aq}^- sensitizer from UV light by DOM chromophores, (2) DOM molecules acting as a scavenger of e_{aq}^-, or (3) through the production of e_{aq}^--quenching reactive oxygen species (e.g., $^\bullet OH$, $^1O_2$, or H_2O_2) by DOM photolysis.[142] Interestingly, in the UV/iodide system,[58] Aldrich Humic Acid enhanced the degradation and defluorination rate of PFOS when present at ≤10 mg/L, but it had an inhibitory effect at 30 mg/L. Sun et al. provided several hypotheses for this enhancement,[58] including the possibility that phenolic electron donors reduce photochemically formed reactive iodine species (I_2, I_3^-) back to I^-, thereby decreasing the e_{aq}^- scavenging by these species (eq 2.15−2.17). Although DOM also generates e_{aq}^-, this pathway is likely an insignificant source of e_{aq}^- in UV-ARP due to its low quantum yield ($\Phi_{e_{aq}^-} \sim 10^{-5}$).[143] Further research is needed to identify the role of DOM in UV-ARP treatment of PFAS, especially in terms of e_{aq}^- scavenging and potential DOM-PFAS interactions.[58,144]

One of the more significant factors influencing PFAS degradation efficiencies is solution pH. Multiple studies have

reported a clear trend of increasing degradation rates and improved defluorination percentages with increasing pH for perfluorocarboxylic acids and perfluorosulfonates,[2,122] with parent contaminant abatement defluorination percentages being especially rapid at pH 12.[33,79] The $[H^+]$ influences multiple aspects of UV-ARP systems, including e_{aq}^- production from the sensitizer (see section 2.3), e_{aq}^- scavenging (see Table 1 and eq 2.14), and secondary chemistry following the initial PFAS-e_{aq}^- reduction event. Scavenging of e_{aq}^- by H^+ does not contribute significantly to $\sum_i k_{S_i,e_{aq}^-}[S_i]_t$ at pH 7 or higher (Figure 4). At circumneutral pH, HSO_3^- quenching reaction may be the main e_{aq}^- scavenger in UV/sulfite ARP,[48] where scavenging by H^+ should be minimal. In addition, HSO_3^- has a low quantum yield of e_{aq}^- generation, so e_{aq}^- formation rates in the UV-sulfite system will be reduced with decreasing pH. Finally, it is interesting to observe the pH dependence of $\gamma_{e_{aq}^-,X^-}$ values for halobenzenes and chloro-substituted anilines (Figure 12), in light of the discussion above on the effect of pH on the DHEH mechanism for reductive PFAS defluorination.

3.2.3.3. Nonhomogeneous UV-ARP. So far, we have discussed UV-ARP studies in which e_{aq}^- and PFAS are homogeneously distributed throughout aqueous solution. An alternative approach that has received attention recently is to enhance PFAS transformation by creating a microheterogeneous system.[25−28] In principle, these microheterogeneous reactors enhance the rate of reductive defluorination relative to the homogeneous system by bringing the e_{aq}^- and PFAS in closer proximity, thereby increasing the frequency of e_{aq}^--PFAS reactions (Figure 17).
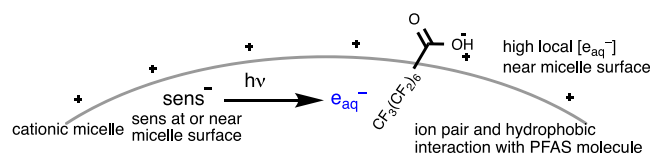

Figure 17. Illustration of the microheterogeneous reductive defluorination of perfluorooctanoic acid (PFOA) via a cationic micelle with a negatively charged hydrated electron sensitizer.

Reported UV-ARP microheterogeneous technologies include UV/organomontmorillonite clay and UV/micelle systems, both of which use indoleacetic acid as the e_{aq}^- sensitizer.[25,26,28,29] The UV/organomontmorillonite clay system works by first adsorbing indoleacetic acid and PFAS on the cationic clay surface.[25,26] Tian et al. demonstrated that the UV/organomontmorillonite clay system allows indoleacetic acid to generate e_{aq}^- and radical cations within the clay layer.[25] This system increased the reductive defluorination of PFOA from approximately 20% (PFOA and indoleacetic acid only, no different from direct photolysis control) to 90% (PFOA, indoleacetic acid, and organomontmorillonite clay) in 10 h. The authors suggested that the clay system further stabilized the radical cations produced from 3-indoleacetic acid and thus minimized radical cations recombination with e_{aq}^-.[25] In the UV/micelle system, a self-assembled micelle was created by a cationic surfactant (e.g., cetyltrimethylammonium bromide), indoleacetic acid (the e_{aq}^- sensitizer), and PFOA.[28] The self-assembled micelle increased the reductive defluorination of PFOA from approximately 10% (PFOA and indoleacetic acid only) to 90% (PFOA, indoleacetic acid, and cationic surfactant) in 2.5 h. Both microheterogeneous technologies demonstrate enhanced reductive defluorination

kinetics when compared to the homogeneous UV/sensitizer system. Both technologies also reduce the e_{aq}^- scavenging impacts of H^+, allowing treatment over a wider range of pH conditions (pH 4 to 8). Chen et al. found that the UV/micelle system could still be effective for PFOA transformation in the presence of high ionic strength and low concentrations of fulvic acid (1 mg/L).[27]

A related microheterogeneous approach is the combination of electrochemical and UV methods for ARP degradation of PFAS. Recent work by Rao et al. demonstrated that PFAS defluorination by e_{aq}^- is enhanced by PFAS sorption to carbon nanotube electrodes at low applied potentials (−0.58 V vs Ag/AgCl).[74] It was hypothesized that this reaction occurs via a two-electron process in which the first electron (derived from the cathode) reduces the C−F bond strength, thereby allowing the second electron (from VUV photolysis of water) to more effectively defluorinate the PFAS than UV treatment alone. In this combined electrochemical/photochemical ARP, PFAS defluorination exhibited a chain-length dependence similar to UV-ARP, with degradation rates of perfluorocarboxylic acids being relatively independent of chain length compared to perfluorosulfonates.[1,30,34]

While these microheterogeneous reactors appear promising for enhanced PFAS treatment, additional research is needed to investigate the application of these systems in actual surface-and groundwater matrices, especially given the impact of water matrix components (e.g., nitrate, DOM) that could also interact with micelles, minerals, and carbon nanotube electrode materials. It is challenging to compare the treatment effectiveness between microheterogeneous systems as experimental conditions vary significantly. Future research should explore utilizing a probe compound to measure key parameters such as $R_f^{e_{aq}^-}$, $[e_{aq}^-]$, and $k'_{S,t}$ to compare between systems.

3.3. Knowledge Gaps

Although UV-ARP have been studied for the e_{aq}^--based transformation of organic and inorganic compounds has been studied for over a decade, several knowledge gaps are still apparent.

3.3.1. Degradation Byproducts.
A question that all degradative advanced water treatment technologies need to address is "are the target contaminants completely mineralized and, if not, are the end products more toxic, less toxic, or just as toxic as initial substrate?" UV-ARP processes also need to address this question. Given the focus on halogen-containing contaminants, the goal of UV-ARP is not complete mineralization but to reduce all halogens to a −1 oxidation state. For inorganic oxyanions, the reaction pathways are well established, with each e_{aq}^- reaction leading to successive reduction of the central atom; for example, bromate can be reduced all the way to bromide given sufficient e_{aq}^- exposure.[117] More work is needed to establish the operating conditions required to achieve the e_{aq}^- exposure necessary for complete transformation of the less-reactive ClO_4^- to Cl^- ion.

Haloaliphatic compounds react by reductive electron capture according to eqs 3.2 and 3.3, the products of which are X^- and a carbon-centered radical ($R^\bullet$). Halogen atoms will be the main site of e_{aq}^- reactivity until all C−X bonds are reduced, with the fate of the carbon centered radical being highly dependent on the water matrix. The reaction pathways for haloaromatic compounds are also established, with halides being produced upon reductive electron capture by the aromatic ring.[136] The secondary chemistry of the aromatic is dependent on additional
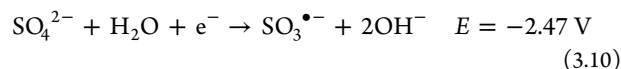
(nonhalogen substituents). For example, e_{aq}^- reduction of chlorophenol is believed to produce phenoxy radicals.[135] Nonhalogenated organic products (e.g., phenol) tend to be less reactive with e_{aq}^- and thus more persistent following dehalogenation of the initial contaminant. For halogenated aromatic and aliphatic compounds, a remaining knowledge gap is the ultimate fate of nonhalogenated end products.

As highlighted herein, recent reports have demonstrated that a variety of PFAS structures (see Figure 14) can be degraded with near 100% defluorination by sequential UV-ARP and oxidation reactions. Continued research efforts are needed to evaluate how these proposed treatment schemes are impacted by water matrix components such as dissolved organic matter.

3.3.2. Role of Additional Reactive Species in UV-ARP Systems.
Prior literature indicates that reactive species other than e_{aq}^- may play an important role in contaminant degradation in UV-ARP.[22,108,145−149] For example, $SO_3^{\bullet-}$ was hypothesized to be responsible for the transformation of vinyl chloride at acidic pH, resulting in a lower percentage dechlorination than obtained using e_{aq}^-.[108] This observation is consistent with the view of Neta and Huie[150] who suggested that $SO_3^{\bullet-}$ may act as a mild oxidant (eq 3.9)

$$SO_3^{\bullet-} + e^- \rightarrow SO_3^{2-} \quad E = 0.63 \text{ V} \tag{3.9}$$
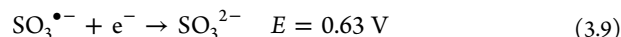
or strong reductant (eq 3.10)

$$SO_4^{2-} + H_2O + e^- \rightarrow SO_3^{\bullet-} + 2OH^- \quad E = -2.47 \text{ V} \tag{3.10}$$

where E is the reduction potential vs NHE. Equation 3.10 demonstrates that $SO_3^{\bullet-}$ has a potential comparable to that of e_{aq}^- (−2.9 V). Based on computational chemistry estimates of one-electron reduction potentials of perfluoropentanoic acid and perfluorobutanesulfonate made by Van Hoomissen and Vyas ($E < -2.0$ V),[141] reductive defluorination of PFAS by $SO_3^{\bullet-}$ should be thermodynamically feasible. Future research should evaluate this possibility.

The superoxide radical anion ($O_2^{\bullet-}$) is another reactive species of interest in e_{aq}^--based UV-ARP[145] since this species is formed by reaction of O_2 with e_{aq}^-. There is disagreement in the literature about the role of $O_2^{\bullet-}$ in the degradation of perfluorocarboxylic acids (like PFOA[146−148]), with some reports suggesting that $O_2^{\bullet-}$ can displace fluorine in C−F bonds yielding F^-. Yet other studies demonstrate that $O_2^{\bullet-}$ is completely unreactive with PFOA.[149] The latter conclusion is consistent with the low oxidation potential of $O_2^{\bullet-}$ ($E = 0.16$ V) and low nucleophilicity of $O_2^{\bullet-}$ in water.[151] The UV-ARP studies employing e_{aq}^- surveyed in this Review indicate that $O_2^{\bullet-}$ is not involved in the reductive defluorination of PFAS. If it were, then significant PFAS abatement should be expected in UV-ARP systems containing dissolved oxygen. However, this is not the case; for example, Qu et al. observed minimal changes in PFOA concentration when continuously sparging O_2 (which should favor $O_2^{\bullet-}$ formation) in the UV/iodide ARP over a 10 h irradiation period.[22]

3.3.3. Availability of Hydrated Electron Bimolecular Rate Constants.
Bimolecular rate constants for e_{aq}^- and many of the organic and inorganic contaminants listed in Table 3 are widely available. There are at least two circumstances in which this is not the case. First, some e_{aq}^- reactions with contaminants (e.g., perchlorate), background scavengers (e.g., bicarbonate), or e_{aq}^- sensitizers (e.g., sulfite) have reported rate constant values that can be considered only as upper limits. This situation arises when the species of interest is "unreactive" toward e_{aq}^-, which

makes the transient absorption monitoring of e_{aq}^- more subject to errors from e_{aq}^- reactive impurities present in either the solvent used (i.e., pure water) or the added chemical solutes.[8] The importance of these slow-reacting species in the total scavenging capacity will increase with increasing e_{aq}^- exposure as more reactive e_{aq}^- scavengers are abated. Thus, the lack of solid e_{aq}^- bimolecular rate constants for these species limits estimation of the scavenging capacity under these conditions.

Second, although many studies have demonstrated reductive defluorination of diverse PFAS structures by UV-ARP, *absolute* bimolecular rate constants for e_{aq}^--PFAS reactions are limited. For the few values that have been reported, there is substantial variability between different studies, even when using the same experimental methods (Table 4). For example, Huang et al.

Table 4. Summary of Literature Hydrated Electron (e_{aq}^-) Bimolecular Rate Constants for Per- And Polyfluoroalkyl Substances (PFAS)

compd	acronym (chain length)	biomolecular rate constant, k (M^{-1}s^{-1})	method	ref
trifluoroacetic acid	TFA (2C)	1.9×10^6	LFP[a,b]	152
		5.0×10^8	LFP[a]	132
perfluoropropanoic acid	PFPrA (3C)	5.8×10^8	LFP[a]	132
perfluorobutanoic acid	PFBA (4C)	7.1×10^6	LFP[a,b]	152
		5.4×10^8	LFP[a]	132
perfluoropentanoic acid	PFPA (5C)	5.2×10^8	LFP[a]	132
perfluorohexanoic acid	PFHxA (6C)	5.4×10^8	LFP[a]	132
perfluoroheptanoic acid	PFHpA (7C)	7.5×10^8	LFP[a]	132
perfluoroocatanoic acid	PFOA (8C)	1.7×10^7	LFP[a]	152
		5.1×10^7	PR[c]	153
		7.1×10^8	LFP[a]	132
perfluorononanoic acid	PFNA (9C)	6.4×10^8	LFP[a]	132
perfluorobutanesulfonate	PFBS (4C)	1.8×10^9	LFP[a]	132
perfluorohexanesulfonate	PFHxS (6C)	1.7×10^9	LFP[a]	132
perfluorooctanesulfonate	PFOS (8C)	2.4×10^9	LFP[a]	132
		7.3×10^7	PR[c,d]	153

[a]Laser flash photolysis, $K_4Fe(CN)_6$ as e_{aq}^- sensitizer, transient absorption monitoring of e_{aq}^-. [b]Corrected to zero ionic strength. [c]Pulse-radiolysis generation of e_{aq}^-, transient absorption monitoring of e_{aq}^-. [d]Measured at concentration greater than critical micellular concentration.

using laser flash photolysis and potassium ferricyanide ($K_4Fe-(CN)_6$) as an e_{aq}^- sensitizer reported bimolecular rate constants for e_{aq}^- and PFCA of $\sim 10^{6-7}$ M^{-1} s^{-1} (1.7×10^7 M^{-1} s^{-1} for PFOA).[152] A recent report by Maza et al. employed the same e_{aq}^- sensitizer and detection method but measured much faster rate constants, not only for perfluorocarboxylic acids (6.4×10^8 M^{-1} s^{-1} for PFOA) but also for perfluorosulfonates (2.4×10^9 M^{-1} s^{-1} for PFOS).[132] A pulse-radiolysis study measured PFOA-e_{aq}^- and PFOS-e_{aq}^- bimolecular rate constants of 5.1×10^7 and 7.3×10^7 M^{-1} s^{-1},[153] respectively. The pulse radiolysis values are faster than the value measured by Huang et al.[152] but still an order of magnitude slower than measured by Maza et al.[132]

It is difficult to understand the wide variability in these reported values between different studies using similar experimental approaches. This was noted by Maza et al. in their recent study,[132] who commented that the reason for the discrepancy was not immediately apparent and probably not due to differences in ionic strength, which tend to produce only small differences in e_{aq}^- bimolecular rate constants within the ranges studied (see also Figure 3). Maza et al. did point out that Huang et al. did not report their range of [PFOA] used in their study, which could have facilitated a closer comparison. It is interesting to note, however, that the e_{aq}^- bimolecular rate constant measured for trifluoroacetic acid by Huang et al. (1.9×10^6 M^{-1} s^{-1}) agrees with the upper limit reported previously by Anbar and Hart ($<1.4 \times 10^6$ M^{-1} s^{-1}[191]), whereas Maza et al.'s value is 2 orders of magnitude faster (5.0×10^8 M^{-1} s^{-1}). One potential reason for this scatter could be the level of residual $[O_2]$ in these solutions; as noted previously, some dissolved oxygen remains no matter what deaeration techniques are used. This $[O_2]$ might not have been consistent between studies. Based on the fast rate constant of O_2 reduction, even micromolar levels will dominate the PFAS-e_{aq}^- chemistry. Alternatively, the PFAS purity might be different, with even trace impurities impacting the PFAS reduction chemistry. However, the disparate values for trifluoroacetic acid suggest that the variability in e_{aq}^- bimolecular rate constants for longer chain PFAS are not caused by the presence of branched isomers, which tend to be more reactive with e_{aq}^-.[34]

Practically, if values from the recent report by Maza et al.[132] are correct and e_{aq}^- rate constants are on the order of 10^8-10^9 M^{-1} s^{-1}, then it is difficult to understand the slow degradation kinetics of PFAS in UV-ARP systems. These data suggest that there is a need to resolve the uncertainty in absolute e_{aq}^- bimolecular rate constants for PFAS.

For PFAS, recommended approaches to measuring e_{aq}^- bimolecular rate constants, such as laser flash photolysis or pulse radiolysis, are only possible for those compounds that have high-purity sources at high concentrations. This represents a small number of the thousands of relevant PFAS structures that may be present in contaminated waters. Another consideration is the isomeric form of the compound of interest. Branched PFAS isomers are known to be much more reactive with e_{aq}^-,[34] and varying percentages of branched isomers have been quantified in commercially available PFAS reagents.[154] If branched and linear isomers are present, then measured e_{aq}^- bimolecular rate constants will represent an average of individual values weighted by the fractional composition of each isomer.

One path forward apart from experimental methods is the use of computational chemistry tools for the prediction of e_{aq}^- bimolecular rate constants. This could include the use of quantitative structure−activity relationships (QSARs) to relate known e_{aq}^- rate constants to molecular descriptors calculated by quantum chemical techniques. Li et al. recently employed this approach and found that the energy of the lowest unoccupied molecular orbital (E_{LUMO}) was a good predictor of k_{TC,e_{aq}^-}.[100,101] Similarly, for hydroxyl radical reactions, density functional theory (DFT)-based methods have been used by Minakata et al. to calculate the aqueous-phase free energies of activation,[155] which in turn were correlated to measured bimolecular reaction rate constants through linear free energy relationships. This latter approach has been utilized extensively for UV-AOP but has not yet been applied to UV-ARP, highlighting this possible area for future research.

3.3.4. Fluoride Yields during Reductive Defluorination of PFAS.

The efficiency of defluorination of PFAS by e_{aq}^- is limited by three main factors: (1) the amount of e_{aq}^- generated for the reaction, (2) the fraction of e_{aq}^- reacting with PFAS relative to water matrix species, and (3) the yield of fluoride per e_{aq}^--PFAS reaction event. This latter probability can be described as a fluoride ion yield. Despite the importance of these yields, no data have been reported for e_{aq}^--PFAS reactions. Acquiring these data are important, because the fluoride ion yield describes the intrinsic limits of e_{aq}^--based PFAS transformation efficiency. It is important to note that the commonly reported percent defluorination (number of F^- produced per total F in parent PFAS) is different from the fluoride yield as it does not account for the reaction efficiency. This is illustrated by the equations below for the two terms. For % defluorination (deF%)

$$\text{deF\%} = \frac{[F^-]}{[PFAS]_0 \times N_{C-F}} \qquad (3.11)$$

where $[F^-]$ is the molar fluoride concentration at the end of the UV-ARP, $[PFAS]_0$ is the initial molar concentration of the parent PFAS, and N_{C-F} is the number of C–F bonds in the parent compound. When using steady-state gamma radiolysis, the fluoride yield is calculated as

$$\gamma_{e_{aq}^-,F^-} = \frac{G_{F^-}}{G_{e_{aq}^-}} \qquad (3.12)$$

where G_{F^-} and $G_{e_{aq}^-}$ are the radiolysis yields of fluoride (unknown) and e_{aq}^- (0.27 μmol Gy^{-18}), respectively. The assumption in eq 3.12 is that all e_{aq}^- formed in the system are scavenged by the PFAS. This typically requires high concentrations of reagents (millimolar) so that all radiolytically formed e_{aq}^- are scavenged by the added substrate, in which case it is important that the reagents are free as possible from e_{aq}^--reactive impurities. To isolate e_{aq}^- reactions, solutions can be spiked with an alcohol such as *tert*-butanol (to scavenge •OH), sparged with N_2 (to limit the e_{aq}^--O_2 reaction), and aliquots withdrawn at varying time intervals (irradiation doses) to measure the concentration of target contaminant and/or transformation product(s).

Apart from radiolysis methods, it may be possible to estimate $\gamma_{e_{aq}^-,F^-}$ from UV/sulfite PFAS transformation data. Using this approach, $\gamma_{e_{aq}^-,F^-}$ can be calculated from the ratio of the e_{aq}^- formation rate ($R_{f,t=0}^{e_{aq}^-}$) and rate of fluoride ion formation ($R_{f,t=0}^{F^-}$), the latter of which can be obtained from the commonly reported deF%. We used the PFOA deF% data from Bentel et al.[30] to calculate $R_{f,t=0}^{F^-}$ and then calculated $R_{f,t=0}^{e_{aq}^-}$ from Figure 8 (similar reactors, sulfite concentrations, and lamp wattages were used) to estimate $\gamma_{e_{aq}^-,F^-}$ for PFOA (eqs 3.13–3.15):

$$\gamma_{e_{aq}^-,F^-} = \frac{R_f^{F^-}}{R_f^{e_{aq}^-}} \qquad (3.13)$$

$$R_f^{F^-} = \frac{\text{deF\%}/100 \times [PFOA]_0 \times N_{C-F}}{\Delta t} = \frac{0.28 \times 25\,\mu M \times 17}{3.9\,h}$$

$$= 31\,\mu M\,h^{-1} \text{ or } 8.5 \times 10^{-9}\,M\,s^{-1} \qquad (3.14)$$

$$\gamma_{e_{aq}^-,F^-} = \frac{8.5 \times 10^{-9}\,M\,s^{-1}}{1.6 \times 10^{-7}\,M\,s^{-1}} = 0.053 \qquad (3.15)$$

The low fluoride ion yield calculated here for PFOA is based on several assumptions (e.g., all e_{aq}^- are scavenged by 25 μM PFOA) and future research measuring fluoride yields from PFAS of diverse structure is needed. Further, given the pH-dependence of halide ion yields for halobenzenes and haloanilines (Figure 13), it is possible that a similar trend of increasing yield with increasing pH could be occurring for PFAS defluorination. Acquiring these yields for different PFAS would enhance our understanding of the reductive defluorination chemistry.

4. SYNTHESIS OF EXISTING INFORMATION TO OPTIMIZE UV-ARP TREATMENT

Development of an optimized UV-ARP system for e_{aq}^--based contaminant transformation is needed to advance these technologies. The above sections have reviewed literature on e_{aq}^- generation (in terms of the specific sensitizer) and e_{aq}^- scavenging in UV-ARP systems. The following optimized experimental conditions were common to all substrates reviewed.

- **Sensitizer selection:** Sulfite is the most used sensitizer and appears to have the optimal benefits for UV-ARP treatment. A concentration of ~10−15 mM likely provides the maximum level of e_{aq}^- generation

- **pH conditions:** Maintaining a pH above 7 is highly desired to mitigate the impact of scavenging by H$^+$ while maintaining at least 2 pH units above 7 when using sulfite as a sensitizer is essential to eliminate the scavenging impact of HSO$_3^-$.[48] UV/sulfite treatment at pH 11−12 seems especially rapid for PFAS and perchlorate, and it would expedite treatment if pH adjustment is feasible.[123]

- **Minimizing scavengers:** For substrates with a fast-biomolecular rate constant ($\geq 10^9$ M^{-1} s^{-1}), it is important to remove dissolved oxygen and minimize other scavengers with fast biomolecular rate constants (e.g., NO$_3^-$, NO$_2^-$). Additional research is necessitated to optimize UV-ARP treatment for real-world waters with DOM and to evaluate the impacts of changing water background matrix conditions on substrate degradation.

Recent PFAS treatment literature has focused on the electrical energy per order (E_{EO}) as a metric for comparing degradative technologies.[32,156] E_{EO} is defined as the energy needed to reduce the concentration of contaminant by 1 order of magnitude in 1 m^3 of water.[157] Comparing E_{EO} values between different UV-ARP systems in this way reveals the differences in efficiency of these processes. For example, although the microheterogeneous UV/indoleacetic acid/micelle system reported recently was described as "efficient," a very high-powered lamp (500 W) was used to treat only 10 mL of solution,[28] resulting in a high E_{EO} (Table 5). A recent study by Liu et al. combined nanofiltration (NF) with UV-sulfite treatment at the pilot scale and found an E_{EO} of 3.7 kWh m^{-3} for PFOA,[32] which is approximately 4-fold lower than the E_{EO} for PFOA in a bench-scale photochemical system (15.8 kWh m^{-3}) reported by Bentel et al.[30,31] The much lower value reported by Liu et al. results from the fact that they considered the total volume of water treated in the NF-UV/sulfite process, which was approximately an order of magnitude greater than the volume treated by UV-sulfite. E_{EO} values for PFOA treatment via UV-ARP in Table 5 tend to be lower than most other degradative technologies.[156] UV-ARP at pH 12.0 is comparable in efficiency to electrochemical oxidation; for example, electrochemical oxidation with a Ti$_4$O$_7$ electro-

Table 5. Electrical Energy per Order (E_{EO}) for the Degradation of Perfluorooctanoic Acid (PFOA) for Different UV-ARP

technology	E_{EO} (kWh/m^3)^a	ref
UV/sulfite, pH 12.0, 18 W, 600 mL, k_{obs} = 4.4 h^{-1} (bench)	15.8	79
UV/sulfite, pH 11.2, 1320 W, 568 L, k_{obs} = 1.5 h^{-1} (pilot)	3.7	32
UV/indoleacetic acid/micelle, 500 W lamp, 10 mL treated, k_{obs} = 1.7 h^{-1} (bench)	67 600	28

$^a E_{EO}$ calculated as E_{EO} = 2.303/k_{obs} × power/volume, where k_{obs} (h^{-1}) is the first-order rate constant, power is the lamp power in kW, and volume is the treated volume in m^3.

chemical membrane yielded E_{EO} values of 5.1 and 6.7 kWh m^{-3} for PFOA and PFOS, respectively.[156]

Minimizing the background scavenging of e_{aq}^- by water matrix components will enhance [e_{aq}^-] and thereby increase the rate of target contaminant degradation. Such minimization may only be important when the treatment time scale is short (less than a few hours). For example, e_{aq}^--based transformation of PFAS occurs over a period of >12 h during which fast-reacting e_{aq}^- scavengers (e.g., O_2, NO_3^-) will be abated quickly through their reaction with e_{aq}^-. Additional background scavengers with slow bimolecular rate constants, such as HCO_3^- and CO_3^{2-}, may become more impactful for PFAS treatment in groundwater systems with high alkalinity, as these compounds become the main scavengers once the fast-reacting e_{aq}^- scavengers are removed. Liu et al. recently employed nanofiltration (NF) to remove PFAS from contaminated groundwater while concomitantly producing a concentrated waste stream that was treated by UV-sulfite.[32] The advantage of NF compared to other membranes like reverse osmosis is that NF does not substantially concentrate ions like nitrate and nitrite.[158] Thus, concentrating PFAS in a small-volume waste stream while at the same time not concentrating e_{aq}^- scavengers would effectively treat more mass per unit time than if the UV-ARP were applied to the contaminated groundwater directly.

Another way to optimize the rate of target contaminant degradation in UV-ARP is to increase the rate of e_{aq}^- formation. This can be done by selecting sensitizers with a higher e_{aq}^- quantum yield or by increasing the fraction of incoming photons absorbed by the sensitizer. Most e_{aq}^- sensitizers absorb in the UV region of the spectrum, where background absorbance by DOM is significant. However, an alternative approach developed by Goez and co-workers is to utilize visible-absorbing e_{aq}^- sensitizers.[159] These visible-absorbing e_{aq}^- generation systems utilize low-cost green light emitting diodes, a ruthenium catalyst ([Ru(bpy)$_3^{2+}$]), and ascorbate (Asc^{2-}) as the electron donor. Following absorption, [Ru(bpy)$_3^{2+}$] rapidly forms a triplet metal-to-ligand charge transfer state that oxidizes Asc^{2-}. The one-electron reduction product of [Ru(bpy)$_3^{2+}$] is encapsulated in a cationic micelle, which facilitates lifetimes long enough to undergo another green photon absorption, thereby producing e_{aq}^- and reforming ground state [Ru(bpy)$_3^{2+}$]. This photocatalyst system demonstrates one possible route toward a more energy-efficient generation of e_{aq}^- by using a green light emitting diode; however, it is not practical for water treatment at this stage given the need for a transition-metal-containing catalyst and self-assembled cationic micelle. Future research efforts to generate visible-absorbing e_{aq}^- sensitizers could improve the energy efficiency of UV-ARP.

5. OUTLOOK AND RECOMMENDATIONS FOR FUTURE RESEARCH

UV-ARP technologies offer a unique advantage to treating recalcitrant chemical contaminants in water that are resistant to UV-AOP or other oxidative processes. Numerous UV-ARP studies have demonstrated effective degradation of oxyanions, high valence transition metals, disinfection byproducts, and PFAS. Yet, the utilization of these technologies in real-world waters is limited. Based on this review of the UV-ARP research, we suggest the following research needs and opportunities to advance UV-ARP research and clarify the role of this technology in water treatment. Note that these research needs are discussed in depth in sections 2.4 and 3.3.

- **Create standard methods for measuring e_{aq}^- in UV-ARP.** Future research should focus on developing a probe compound capable of quantifying photochemical parameters important in UV-ARP, such as [e_{aq}^-], background e_{aq}^- scavenging capacity, and rates of e_{aq}^- formation. The deployment of a probe compound will provide researchers a way to compare treatment effectiveness between studies and optimize treatment in real-world waters. Measuring the [e_{aq}^-] will also facilitate modeling target contaminant transformation rates in UV-ARP.

- **Understand the role of DOM.** The impact of DOM on the e_{aq}^- scavenging capacity and light absorbing capacity in UV-ARP systems needs further investigation. Future research should aim to determine e_{aq}^- biomolecular rate constants for DOM and the impact of e_{aq}^- exposure on DOM's absorbance. Addressing these research gaps will help to evaluate the impact of DOM on UV-ARP treatment of real-world waters where DOM is an important e_{aq}^- scavenger and light absorber.

- **Clarify the role of additional reactive species in UV-ARP.** Studies have suggested that $SO_3^{\bullet-}$ contributes to target contaminant transformation in the UV/sulfite system, for example, perchlorate and nitrate. Future research should explore whether reactions with $SO_3^{\bullet-}$ contribute to the reductive defluorination of PFAS. This reaction is thermodynamically favorable based on the reduction potentials of $SO_3^{\bullet-}$ (experimental)[150] and perfluorobutanesulfonate (computational).[141] Direct, time-resolved kinetic measurements of bimolecular rate constants between PFAS and $SO_3^{\bullet-}$ could help answer this question. A computational assessment of the reactivity between PFAS and $SO_3^{\bullet-}$ may also provide insight.

- **Resolve the uncertainty in e_{aq}^- bimolecular rate constants for PFAS.** There is an abundance of bimolecular rate constants for e_{aq}^- and various organic and inorganic contaminants. PFAS are an exception to this, however, due the large number of PFAS and the difficulty of obtaining high quantities of pure compounds needed for e_{aq}^- kinetic experiments. In addition, available PFAS-e_{aq}^- rate constants in the literature are highly variable (k = 10^7−10^9 M^{-1} s^{-1} for PFOA; see Table 4), and thus, the intrinsic reactivity of PFAS with e_{aq}^- is still a major knowledge gap. Future work should investigate this discrepancy, potentially by incorporating the reaction yield (eq 3.12), as has been done previously for halogenated aromatic compounds (e.g., Figures 11 and 12). We suggest that direct, time-resolved methods such as laser flash photolysis and pulse radiolysis be employed for measuring e_{aq}^- bimolecular rate constants given the

complex background photochemistry occurring with e_{aq}^- sensitizers. In addition, computational chemistry approaches should be explored to discern structural trends in biomolecular rate constants with the more than thousands of relevant PFAS structures that may be present in contaminated waters.

- **Determine PFAS fluoride yields.** Quantifying the fluoride ion yield for e_{aq}^--PFAS reactions is important, as it describes the intrinsic limits of e_{aq}^--PFAS transformation efficiency. Equation 3.12 demonstrates how these values can be obtained from steady-state gamma radiolysis experiments. While steady-state gamma radiolysis is our recommended method for measuring these values, other experimental approaches may be possible. For example, the preliminary calculations presented above using UV/sulfite data suggest that the fluoride ion yield for PFOA is $\approx 5\%$. Future work to verify this value and expand fluoride yield measurements to additional PFAS structures is needed.

We would like to conclude by giving some final thoughts on the question of whether there is there any practical role for UV-ARP in water treatment. This question is important considering the attention given to UV-ARP for treatment of PFAS. While e_{aq}^--based processes appear to be one of the more promising methods for PFAS transformation, it is difficult to see how UV-ARP could be implemented at the same scale as UV-AOP. The main barriers include the large UV doses required, the undesirable byproducts from e_{aq}^- sensitizers in the treated water, and the rapid scavenging of e_{aq}^- by O_2. The use of UV-ARP for contaminant treatment appears to be most promising for groundwater applications with low background e_{aq}^- scavengers (e.g., little to no dissolved oxygen or nitrate present). Alternatively, the treatment of small volumes of concentrated contaminant waste streams, like from NF, RO filtration or ion exchange, could justify the large energy requirements of UV-ARP. Additional applications could include modular pump and treat systems for contaminated sites or temporary cleanup from chemical spills. Exploring these UV-ARP applications requires continued bench level experiments and more emphasis on pilot studies. Future research should seek to determine where UV-ARP and other e_{aq}^--based treatment schemes fit into the management of chemical contaminants in water, most notably PFAS.

■ ASSOCIATED CONTENT

Ⓢ Supporting Information

The Supporting Information is available free of charge at https://pubs.acs.org/doi/10.1021/acsenvironau.1c00042.

Excel sheets containing bimolecular rate constants for hydrated electron reaction with organic compounds and a summary of UV-ARP treatment literature (XLSX)

■ AUTHOR INFORMATION

Corresponding Author

Garrett McKay − *Zachry Department of Civil & Environmental Engineering, Texas A&M University, College Station, Texas 77843, United States;* ⓞ orcid.org/0000-0002-6529-0892; Phone: 979-458-6540; Email: gmckay@tamu.edu

Authors

Benjamin D. Fennell − *Zachry Department of Civil & Environmental Engineering, Texas A&M University, College Station, Texas 77843, United States*

Stephen P. Mezyk − *Department of Chemistry and Biochemistry, California State University, Long Beach, Long Beach, California 90840, United States*

Complete contact information is available at:
https://pubs.acs.org/10.1021/acsenvironau.1c00042

Notes

The authors declare no competing financial interest.

■ ABBREVIATIONS AND SYMBOLS USED

α	(absorption coefficient of background water matrix, cm^{-1})
$CO_2^{\bullet-}$	(carbon dioxide radical anion)
e_{aq}^-	(hydrated electron)
ε_{sens}	(molar absorption coefficient, $M^{-1}cm^{-1}$)
E_{EO}	(electrical energy per order, kWh m^{-3})
k_d'	(first-order direct photolysis rate constant, s^{-1})
$k_{S,t}'$	(e_{aq}^- scavenging capacity, s^{-1})
$k_{TC,e_{aq}^-}^q$	(bimolecular rate constant for e_{aq}^- quenching by the target contaminant, $M^{-1} s^{-1}$)
$k_{TC,e_{aq}^-}^t$	(bimolecular rate constant for target contaminant transformation, $M^{-1} s^{-1}$)
k_{TC,e_{aq}^-}	(bimolecular target contaminant-hydrated electron rate constant, $M^{-1} s^{-1}$)
I_0	(photon irradiance, mmol photons $cm^{-2}s^{-1}$)
IAA	(3-indoleacetic acid)
$^{\bullet}H$	(hydrogen atom)
l	(path length, cm)
LED	(light emitting diode)
LP-M	(low-pressure mercury lamp)
MP-M	(medium-pressure mercury lamp)
MCAA	(monochloroacetic acid)
NTA	(nitrilotriacetic acid)
$^{\bullet}OH$	(hydroxyl radical)
$\Phi_{e_{aq}^-}$	(quantum yield of e_{aq}^- formation)
PFAS	(per- and polyfluoroalkyl substances)
PFCA	(perfluorocarboxylic acid)
PFECA	(perfluoroethercarboxylic acid)
PFSA	(perfluorosulfonate)
$R_f^{e_{aq}^-}$	(hydrated electron formation rate, M s^{-1})
$R_f^{X^-}$	(halide formation rate, M s^{-1})
sens	(sensitizer)
$SO_3^{\bullet-}$	(sulfite radical anion)
S	(scavenger)
TC	(target contaminant)
UV	(ultraviolet)
UV-ARP	(UV-Advanced Reduction Process)
VUV	(vacuum ultraviolet)
W	(watt)

$\gamma_{e_{aq}^- X^-}$ (halide yield)

■ REFERENCES

(1) Park, H.; Vecitis, C. D.; Cheng, J.; Choi, W.; Mader, B. T.; Hoffmann, M. R. Reductive Defluorination Of Aqueous Perfluorinated Alkyl Surfactants: Effect of Ionic Headgroup and Chain Length. *J. Phys. Chem. A.* **2009**, *113*, 690−696.

(2) Cui, J.; Gao, P.; Deng, Y. Destruction of Per- and Polyfluoroalkyl Substances (PFAS) with Advanced Reduction Processes (ARPs): A Critical Review. *Environ. Sci. Technol.* **2020**, *54* (7), 3752−3766.

(3) Yang, L.; He, L.; Xue, J.; Ma, Y.; Shi, Y.; Wu, L.; Zhang, Z. UV/SO$_3^{2-}$ Based Advanced Reduction Processes of Aqueous Contaminants: Current Status and Prospects. *Chemical Engineering Journal* **2020**, *397*, 125412.

(4) Kaushik, V.; Duan, Y.; Jung, B.; Batchelor, B.; Abdel-Wahab, A. Arsenic Removal Using Advanced Rreduction Process with Dithionite/UV—A Kinetic Study. *Journal of Water Process Engineering* **2018**, *23*, 314−319.

(5) Jung, B.; Sivasubramanian, R.; Batchelor, B.; Abdel-Wahab, A. Chlorate Reduction by Dithionite/UV Advanced Reduction Process. *International Journal of Environmental Science and Technology* **2017**, *14*, 123−134.

(6) Botlaguduru, V. S. V.; Batchelor, B.; Abdel-Wahab, A. Application of UV−Sulfite Advanced Reduction Process to Bromate Removal. *Journal of Water Process Engineering* **2015**, *5*, 76−82.

(7) Vellanki, B. P.; Batchelor, B.; Abdel-Wahab, A. Advanced Reduction Processes: A New Class of Treatment Processes. *Environ. Eng. Science* **2013**, *30* (5), 264−271.

(8) Buxton, G. V.; Greenstock, C. L.; Helman, W. P.; Ross, A. B. Critical Review of Rate Constants for Reactions of Hydrated Electrons, Hydrogen Atoms and Hydroxyl Radicals (·OH/·O− in Aqueous Solution. *J. Phys. Chem. Ref. Data* **1988**, *17* (2), 513−886.

(9) Bolton, J. R.; Cater, S. R. Treatment of Contaminated Waste Waters and Groundwaters With Photolytically Generated Hydrated Electrons. US 5,258,124 C1, 1991.

(10) Chen, G.; Hanukovich, S.; Chebeir, M.; Christopher, P.; Liu, H. Nitrate Removal via a Formate Radical-Induced Photochemical Process. *Environ. Sci. Technol.* **2019**, *53* (1), 316−324.

(11) Moussavi, G.; Shekoohiyan, S. Simultaneous Nitrate Reduction and Acetaminophen Oxidation Using the Continuous-flow Chemicalless VUV Process as an Integrated Advanced Oxidation and Reduction Process. *J. Hazard Mater.* **2016**, *318*, 329−338.

(12) Duan, Y.; Batchelor, B. Impacts of Natural Organic Matter on Perchlorate Removal by an Advanced Reduction Process. *J. Environ. Sci. Health A Tox Hazard Subst Environ. Eng.* **2014**, *49* (6), 731−40.

(13) Vellanki, B. P.; Batchelor, B. Perchlorate Reduction by the Sulfite/Ultraviolet Light Advanced Reduction Process. *Journal Hazardous Materials* **2013**, *262*, 348−56.

(14) Liu, X.; Wang, L.; Sun, Z.; Shao, Y.; Yu, T. Treatment of Aqueous Bromate by Supermagnetic BiOCl-Mediated Advanced Reduction Process. *Catalysts* **2017**, *7* (12), 131.

(15) Nawaz, S.; Shah, N. S.; Khan, J. A.; Sayed, M.; Al-Muhtaseb, A. a. H.; Andersen, H. R.; Muhammad, N.; Murtaza, B.; Khan, H. M. Removal Efficiency and Economic Cost Comparison of Hydrated Electron-mediated Reductive Pathways for Treatment of Bromate. *Chemical Engineering Journal* **2017**, *320*, 523−531.

(16) Jung, B.; Nicola, R.; Batchelor, B.; Abdel-Wahab, A. Effect of Low- and Medium-pressure Hg UV Irradiation on Bromate Removal in Advanced Reduction Process. *Chemosphere* **2014**, *117*, 663−72.

(17) Xiao, Q.; Yu, S.; Li, L.; Wang, T.; Liao, X.; Ye, Y. An Overview of Advanced Reduction Processes for Bromate Removal from Drinking Water: Reducing Agents, Activation Methods, Applications and Mechanisms. *J. Hazard Mater.* **2017**, *324* (Pt B), 230−240.

(18) Xiao, Q.; Wang, T.; Yu, S.; Yi, P.; Li, L. Influence of UV Lamp, Sulfur(IV) Concentration, and pH on Bromate Degradation in UV/Sulfite Systems: Mechanisms and Applications. *Water Res.* **2017**, *111*, 288−296.

(19) Xiao, Q.; Yu, S.; Li, L.; Zhang, Y.; Yi, P. Degradation of Bromate by Fe(II)Ti(IV) Layered Double Hydroxides Nanoparticles Under Ultraviolet Light. *Water Res.* **2019**, *150*, 310−320.

(20) Xie, B.; Shan, C.; Xu, Z.; Li, X.; Zhang, X.; Chen, J.; Pan, B. Onestep Removal of Cr(VI) at Akaline pH by UV/Sulfite Process: Reduction to Cr(III) and in situ Cr(III) Precipitation. *Chemical Engineering Journal* **2017**, *308*, 791−797.

(21) Wang, X.; Liu, H.; Shan, C.; Zhang, W.; Pan, B. A Novel Combined Process for Efficient Removal of Se(VI) from Sulfate-rich Water: Sulfite/UV/Fe(III) Coagulation. *Chemosphere* **2018**, *211*, 867−874.

(22) Qu, Y.; Zhang, C.; Li, F.; Chen, J.; Zhou, Q. Photo-reductive Defluorination of Perfluorooctanoic Acid in Water. *Water Res.* **2010**, *44* (9), 2939−47.

(23) Song, Z.; Tang, H.; Wang, N.; Zhu, L. Reductive Defluorination of Perfluorooctanoic Acid by Hydrated Electrons in a Sulfite-mediated UV Photochemical System. *J. Hazard Mater.* **2013**, *262*, 332−8.

(24) Gu, Y.; Liu, T.; Wang, H.; Han, H.; Dong, W. Hydrated Electron Based Decomposition of Perfluorooctane Sulfonate (PFOS) in the VUV/Sulfite System. *Sci. Total Environ.* **2017**, *607−608*, 541−548.

(25) Tian, H.; Gao, J.; Li, H.; Boyd, S. A.; Gu, C. Complete Defluorination of Perfluorinated Compounds by Hydrated Electrons Generated from 3-Indole-Acetic-Acid in Organomodified Montmorillonite. *Sci. Rep.* **2016**, *6*, 32949.

(26) Tian, H.; Gu, C. Effects of Different factors on Photodefluorination of Perfluorinated Compounds by Hydrated Electrons in Organo-montmorillonite System. *Chemosphere* **2018**, *191*, 280−287.

(27) Chen, Z.; Mi, N.; Li, C.; Teng, Y.; Chen, Y.; Gu, C. Effects of Different Variables on Photodestruction of Perfluorooctanoic Acid in Self-assembled Micelle System. *Sci. Total Environ.* **2020**, *742*, 140438.

(28) Chen, Z.; Li, C.; Gao, J.; Dong, H.; Chen, Y.; Wu, B.; Gu, C. Efficient Reductive Destruction of Perfluoroalkyl Substances under Self-Assembled Micelle Confinement. *Environ. Sci. Technol.* **2020**, *54* (8), 5178−5185.

(29) Chen, Z.; Teng, Y.; Mi, N.; Jin, X.; Yang, D.; Wang, C.; Wu, B.; Ren, H.; Zeng, G.; Gu, C. Highly Efficient Hydrated Electron Utilization and Reductive Destruction of Perfluoroalkyl Substances Induced by Intermolecular Interaction. *Environ. Sci. Technol.* **2021**, *55* (6), 3996−4006.

(30) Bentel, M. J.; Yu, Y.; Xu, L.; Li, Z.; Wong, B. M.; Men, Y.; Liu, J. Defluorination of Per- and Polyfluoroalkyl Substances (PFASs) with Hydrated Electrons: Structural Dependence and Implications to PFAS Remediation and Management. *Environ. Sci. Technol.* **2019**, *53* (7), 3718−3728.

(31) Bentel, M. J.; Yu, Y.; Xu, L.; Kwon, H.; Li, Z.; Wong, B. M.; Men, Y.; Liu, J. Degradation of Perfluoroalkyl Ether Carboxylic Acids with Hydrated Electrons: Structure-Reactivity Relationships and Environmental Implications. *Environ. Sci. Technol.* **2020**, *54* (4), 2489−2499.

(32) Liu, C. J.; McKay, G.; Jiang, D.; Tenorio, R.; Cath, J. T.; Amador, C.; Murray, C. C.; Brown, J. B.; Wright, H. B.; Schaefer, C.; Higgins, C. P.; Bellona, C.; Strathmann, T. J. Pilot-Scale Field Demonstration of a Hybrid Nanofiltration and UV-Sulfite Treatment Train for Groundwater Contaminated by Per- and Polyfluoroalkyl Substances (PFASs). *Water Res.* **2021**, *205*, 117677.

(33) Liu, Z.; Bentel, M. J.; Yu, Y.; Ren, C.; Gao, J.; Pulikkal, V. F.; Sun, M.; Men, Y.; Liu, J. Near-Quantitative Defluorination of Perfluorinated and Fluorotelomer Carboxylates and Sulfonates with Integrated Oxidation and Reduction. *Environ. Sci. Technol.* **2021**, *55* (10), 7052−7062.

(34) Tenorio, R.; Liu, J.; Xiao, X.; Maizel, A.; Higgins, C. P.; Schaefer, C. E.; Strathmann, T. J. Destruction of Per- and Polyfluoroalkyl Substances (PFASs) in Aqueous Film-Forming Foam (AFFF) with UV-Sulfite Photoreductive Treatment. *Environ. Sci. Technol.* **2020**, *54* (11), 6957−6967.

(35) Javed, H.; Lyu, C.; Sun, R.; Zhang, D.; Alvarez, P. J. J. Discerning the Inefficacy of Hydroxyl Radicals During Perfluorooctanoic Acid Degradation. *Chemosphere* **2020**, *247*, 125883.

(36) Cao, Y.; Qiu, W.; Li, J.; Jiang, J.; Pang, S. Review on UV/Sulfite Process for Water and Wastewater Treatments in the Presence or Absence of O_2. *Sci. Total Environ.* **2021**, *765*, 142762.

(37) Wu, S.; Shen, L.; Lin, Y.; Yin, K.; Yang, C. Sulfite-based Advanced Oxidation and Reduction Processes for Water Treatment. *Chemical Engineering Journal* **2021**, *414*, 128872.

(38) Trojanowicz, M.; Bojanowska-Czajka, A.; Bartosiewicz, I.; Kulisa, K. Advanced Oxidation/Reduction Processes Treatment for Aaqueous Perfluorooctanoate (PFOA) and Perfluorooctanesulfonate (PFOS) — A Review of Recent Advances. *Chemical Engineering Journal* **2018**, *336*, 170−199.

(39) Liu, X.; Yoon, S.; Batchelor, B.; Abdel-Wahab, A. Photochemical Degradation of Vinyl Chloride with an Advanced Reduction Process (ARP) − Effects of Reagents and pH. *Chemical Engineering Journal* **2013**, *215−216*, 868−875.

(40) Rosenfeldt, E. J.; Linden, K. G. The $R_{OH, UV}$ Concept to Characterize and the Model UV/H_2O_2 Process in Natural Waters. *Environ. Sci. Technol.* **2007**, *41* (7), 2548−2553.

(41) Apell, J. N.; McNeill, K. Updated and Validated Solar Irradiance Reference Spectra for Estimating Environmental Photodegradation Rates. *Environ. Sci. Process Impacts* **2019**, *21* (3), 427−437.

(42) Bolton, J. R.; Mayor-Smith, I.; Linden, K. G. Rethinking the Concepts of Fluence (UV Dose) and Fluence Rate: The Importance of Photon-based Units - A Systemic Review. *Photochem. Photobiol.* **2015**, *91* (6), 1252−62.

(43) Leifer, A. *The Kinetics of Environmental Aquatic Photochemistry Theory and Practice*; American Chemical Society: 1988.

(44) Mack, J.; Bolton, J. R. Photochemistry of Nitrite and Nitrate in Aqueous Solution: A Review. *J. Photochem. Photobiol., A* **1999**, *128* (1−3), 1−13.

(45) Xie, B.; Li, X.; Huang, X.; Xu, Z.; Zhang, W.; Pan, B. Enhanced Debromination of 4-Bromophenol by the UV/Sulfite Process: Efficiency and Mechanism. *J. Environ. Sci. (China)* **2017**, *54*, 231−238.

(46) Yazdanbakhsh, A.; Eslami, A.; Moussavi, G.; Rafiee, M.; Sheikhmohammadi, A. Photo-assisted Degradation of 2, 4, 6-Trichlorophenol by an Advanced Reduction Process Based on Sulfite Anion Radical: Degradation, Dechlorination and Mineralization. *Chemosphere* **2018**, *191*, 156−165.

(47) Nash, K.; Mulac, W.; Noon, M.; Fried, S.; Sullivan, J. C. Pulse Radiolysis Studies of U(VI) Complexes in Aqueous Media. *Journal of Inorganic and Nuclear Chemistry* **1981**, *43* (5), 897−899.

(48) Maza, W. A.; Breslin, V. M.; Plymale, N. T.; DeSario, P. A.; Epshteyn, A.; Owrutsky, J. C.; Pate, B. B. Nanosecond Transient Absorption Studies of the pH-dependent Hydrated Electron Quenching by HSO_3^-. *Photochem. Photobiol. Sci.* **2019**, *18* (6), 1526−1532.

(49) Shetiya, R. S.; Rao, K. N.; Shankar, J. Determination of rate constants for the reactions of H, OH and e aq with indole-3-acetic acid and other plant hormones. *Radiation Effects* **1972**, *14* (3−4), 185−189.

(50) Westerhoff, P.; Mezyk, S.; Cooper, W. J.; Minakata, D. Electron Pulse Radiolysis Determination of Hydroxyl Radical Rate Constants with Suwannee River Fulvic Acid and Other Dissolved Organic Matter Isolates. *Environ. Sci. Technol.* **2007**, *41* (13), 4640−4646.

(51) Wong, G. T. F.; Zhang, L. Chemical Removal of Oxygen with Sulfite for the Polarographic or Voltammetric Determination of Iodate or Iodide in Seawater. *Marine Chemistry* **1992**, *38* (1−2), 109−116.

(52) Brezonik, P. L.; Arnold, W. A. *Water Chemistry: An Introduction to the Chemistry of Natural and Engineered Aquatic Systems*; Oxford University Press, Inc.: 2011.

(53) What are Humic Substances? https://humic-substances.org/ (accessed October 5, 2021).

(54) *NDRL/NIST Solution Kinetics Database on the Web*, 2002 ed.; National Institute of Standards and Technology: Notre Dame Radiation Laboratory, 2021. https://kinetics.nist.gov/solution/ (accessed October 5, 2021).

(55) Trojanowicz, M.; Bobrowski, K.; Szostek, B.; Bojanowska-Czajka, A.; Szreder, T.; Bartoszewicz, I.; Kulisa, K. A Survey of Analytical Methods Employed for Monitoring of Advanced Oxidation/

(56) Reduction Processes for Decomposition of Selected Perfluorinated Environmental Pollutants. *Talanta* **2018**, *177*, 122−141.

(56) Grossweiner, L. I.; Swenson, G. W.; Zwicker, E. F. Photochemical Generation of the Hydrated Electron. *Science* **1963**, *141* (3583), 805−806.

(57) Li, X.; Ma, J.; Liu, G.; Fang, J.; Yue, S.; Guan, Y.; Chen, L.; Liu, X. Efficient Reductive Dechlorination of Monochloroacetic Acid by Sulfite/UV Process. *Environ. Sci. Technol.* **2012**, *46* (13), 7342−9.

(58) Sun, Z.; Zhang, C.; Chen, P.; Zhou, Q.; Hoffmann, M. R. Impact of Humic Acid on the Photoreductive Degradation of Perfluorooctane Sulfonate (PFOS) by UV/Iodide Process. *Water Res.* **2017**, *127*, 50−58.

(59) Sauer, M. C.; Crowell, R. A.; Shkrob, I. A. Electron Photodetachment from Aqueous Anions. 1. Quantum Yields for Generation of Hydrated Electron by 193 and 248 nm Laser Photoexcitation of Miscellaneous Iorganic nions. *Journal Physical Chemistry A* **2004**, *108* (25), 5490−5502.

(60) Yu, K.; Li, X.; Chen, L.; Fang, J.; Chen, H.; Li, Q.; Chi, N.; Ma, J. Mechanism and Efficiency of Contaminant Reduction by Hydrated Electron in the Sulfite/Iodide/UV Process. *Water Res.* **2018**, *129*, 357−364.

(61) Awtrey, A. D.; Connick, R. E. The Absorption Spectra of I_2, I_3^-, I^-, IO_3^-, $S_4O_6^=$ and $S_2O_3^=$. Heat of the Reaction $I_3^- = I_2 + I^-$. *J. Am. Chem. Soc.* **1951**, *73* (4), 1842−1843.

(62) Iwata, A.; Nakashima, N.; Kusaba, M.; Izawa, Y.; Yamanaka, C. Quantum Yields of Hydrated Electrons by UV Laser Irradiation. *Chem. Phys. Lett.* **1993**, *207* (2−3), 137−142.

(63) Deister, U.; Neeb, R.; Helas, G.; Warneck, P. Temperature Dependence of the Equilibrium $CH_2(OH)_2 + HSO_3^- = CH_2(OH)-SO_3^- + H_2O$ in Aqueous Solution. *J. Phys. Chem.* **1986**, *90* (14), 3213−3217.

(64) Sun, Z.; Zhang, C.; Xing, L.; Zhou, Q.; Dong, W.; Hoffmann, M. R. UV/Nitrilotriacetic Acid Process as a Novel Strategy for Efficient Photoreductive Degradation of Perfluorooctanesulfonate. *Environ. Sci. Technol.* **2018**, *52* (5), 2953−2962.

(65) Tian, H.; Guo, Y.; Pan, B.; Gu, C.; Li, H.; Boyd, S. A. Enhanced Photoreduction of Nitro-aromatic Compounds by Hydrated Electrons Derived from Indole on Natural Montmorillonite. *Environ. Sci. Technol.* **2015**, *49* (13), 7784−92.

(66) Kaper, J. M.; Gebhard, O.; Van Den Berg, C. J.; Veldstra, H. Studies on Indolepyruvic Acid. *Arch. Biochem. Biophys.* **1963**, *103* (3), 475−487.

(67) Zechner, J.; Kohler, G.; Getoff, N.; Tatischeff, I.; Klein, R. Wavelength Effects on the Photoprocesses of Indole and Derivatives in Solution. *Photochem. Photobiol.* **1981**, *34* (2), 163−168.

(68) Deister, U.; Warneck, P. Photooxidation of SO_3^{2-} in Aqueous Solution. *J. Phys. Chem.* **1990**, *94*, 2191−2198.

(69) Fischer, M.; Warneck, P. Photodecomposition and Photo-oxidation of Hydrogen Sulfite in Aqueous Solution. *J. Phys. Chem.* **1996**, *100*, 15111−15117.

(70) Lee, J. Y.; Baugher, J. F.; Grossweiner, L. I. Pairwise Recombination in the Decay of Photochemical Hydrated Electrons. *Photochem. Photobiol.* **1979**, *29* (5), 867−874.

(71) Schwarz, H. A.; Gill, P. S. Diffusion-Limited Solvated Electron Reactions in Ethanol and Water. *J. Phys. Chem.* **1977**, *81* (1), 22−25.

(72) Elliot, A. J.; Ouellette, D. C. Temperature Dependence of the Rate Constant for the Reaction $e_{aq}^- + OH$ in Water up to 150 C. *J. Chem. Soc., Faraday Trans.* **1994**, *90* (6), 837−841.

(73) Zoschke, K.; Bornick, H.; Worch, E. Vacuum-UV Radiation at 185 nm in Water Treatment-A Review. *Water Res.* **2014**, *52*, 131−45.

(74) Rao, U.; Su, Y.; Khor, C. M.; Jung, B.; Ma, S.; Cwierny, D. M.; Wong, B. M.; Jassby, D. Structural Dependence of Reductive Defluorination of Linear PFAS Compounds in a UV/Electrochemical System. *Environ. Sci. Technol.* **2020**, *54* (17), 10668−10677.

(75) Rahn, R. O. Potassium Iodide as a Chemical Actinometer for 254 nm Radiation: Use of Iodate as an Electron Scavenger. *Photochem. Photobiol.* **1997**, *66*, 450−455.

(76) Backer, L. C.; Esteban, E.; Rubin, C. H.; Kieszak, S.; McGeehin, M. A. Assessing Acute Diarrhea From Sulfate In Drinking Water. *Journal - American Water Works Association* **2001**, *93* (9), 76−84.

(77) Gu, Y.; Liu, T.; Zhang, Q.; Dong, W. Efficient Decomposition of Perfluorooctanoic Acid by a High Photon Flux UV/Sulfite Process: Kinetics and Associated Toxicity. *Chemical Engineering Journal* **2017**, *326*, 1125−1133.

(78) Gu, Y.; Dong, W.; Luo, C.; Liu, T. Efficient Reductive Decomposition of Perfluorooctanesulfonate in a High Photon Flux UV/Sulfite System. *Environ. Sci. Technol.* **2016**, *50* (19), 10554−10561.

(79) Bentel, M. J.; Liu, Z.; Yu, Y.; Gao, J.; Men, Y.; Liu, J. Enhanced Degradation of Perfluorocarboxylic Acids (PFCAs) by UV/Sulfite Treatment: Reaction Mechanisms and System Efficiencies at pH 12. *Environmental Science & Technology Letters* **2020**, *7* (5), 351−357.

(80) Rosenfeldt, E. J.; Linden, K. G. Degradation of Endocrine Disrupting Chemicals Bisphenol A, Ethinyl Estradiol, and Estradiol during UV Photolysis and Advanced Oxidation Processes. *Environmental science & technology* **2004**, *38* (20), 5476−5483.

(81) Rosenfeldt, E. J.; Linden, K. G.; Canonica, S.; von Gunten, U. Comparison of the Efficiency of ·OH Radical Formation During Ozonation and the Advanced Oxidation Processes O_3/H_2O_2 and UV/H_2O_2. *Water Res.* **2006**, *40* (20), 3695−704.

(82) Burns, J. M.; Cooper, W. J.; Ferry, J. L.; King, D. W.; DiMento, B. P.; McNeill, K.; Miller, C. J.; Miller, W. L.; Peake, B. M.; Rusak, S. A.; Rose, A. L.; Waite, T. D. Methods for Reactive Oxygen Species (ROS) Detection in Aqueous Environments. *Aquatic Sciences* **2012**, *74* (4), 683−734.

(83) Pi, Y.; Schumacher, J.; Jekel, M. The Use of para-Chlorobenzoic Acid (pCBA) as an Ozone/Hydroxyl Radical Probe Compound. *Ozone: Science & Engineering* **2005**, *27* (6), 431−436.

(84) Ulliman, S. L.; McKay, G.; Rosario-Ortiz, F. L.; Linden, K. G. Low Levels of Iron Enhance UV/H_2O_2 Efficiency at Neutral pH. *Water Res.* **2018**, *130*, 234−242.

(85) Ulliman, S. L.; Miklos, D. B.; Hübner, U.; Drewes, J. E.; Linden, K. G. Improving UV/H_2O_2 Performance Following Tertiary Treatment of Municipal Wastewater. *Environmental Science: Water Research & Technology* **2018**, *4* (9), 1321−1330.

(86) Zepp, R. G.; Braun, A. M.; Hoigne, J.; Leenheer, J. A. Photoproduction of Hydrated Electrons From Natural Organic Solutes in Aquatic Environments. *Environ. Sci. Technol.* **1987**, *21* (5), 485−490.

(87) Thomas-Smith, T. E.; Blough, N. V. Photoproduction of Hydrated Electron from Constituents of Natural Waters. *Environ. Sci. Technol.* **2001**, *35* (13), 2721−2726.

(88) Gu, J.; Ma, J.; Jiang, J.; Yang, L.; Yang, J.; Zhang, J.; Chi, H.; Song, Y.; Sun, S.; Tian, W. Q. Hydrated electron (e_{aq}^-) Generation from Phenol/UV: Efficiency, Influencing Factors, and Mechanism. *Applied Catalysis B: Environmental* **2017**, *200*, 585−593.

(89) Li, X.; Fang, J.; Liu, G.; Zhang, S.; Pan, B.; Ma, J. Kinetics and Efficiency of the Hydrated Electron-induced Dehalogenation by the Sulfite/UV Process. *Water Res.* **2014**, *62*, 220−8.

(90) Munch, D. J.; Much, J. W.; Pawlecki, A. M. *Method 552.2 - Determination of Haloacetic Acids and Dalapon in Drinking Water by Liquid-Liquid Extraction, Derivatization and Gas Chromatography with Electron Capture Detection - Revision 1.0*; U.S. Environmental Protection Agency: 1995.

(91) Anbar, M.; Hart, E. J. The Reaction of Haloaliphatic Compounds with Hydrated Electrons. *J. Phys. Chem.* **1965**, *69* (1), 271−274.

(92) Butler, I. B.; Schoonen, M. A.; Rickard, D. T. Removal of Dissolved Oxygen From Water: A Comparison of Four Common Techniques. *Talanta* **1994**, *41* (2), 211−215.

(93) Crittenden, J. C.; Hu, S.; Hand, D. W.; Green, S. A. A Kinetic Model for H_2O_2/UV Process In a Completely Mixed Batch Reactor. *Water Res.* **1999**, *33* (10), 2315−2328.

(94) Zhang, R.; Sun, P.; Boyer, T. H.; Zhao, L.; Huang, C. H. Degradation of Pharmaceuticals and Metabolite in Synthetic Human Urine by UV, UV/H_2O_2, and UV/PDS. *Environ. Sci. Technol.* **2015**, *49* (5), 3056−66.

(95) Ianni, J. C. A Comparison of the Bader-Deuflhard and the Cash-Karp Runge-Kutta Integrators for the GRI-MECH 3.0 Model Based on

the Chemical Kinetics Code Kintecus. In *Computational Fluid and Solid Mechanics 2003*; Bathe, K. J., Ed.; Elsevier Science Ltd: Oxford, 2003; pp 1368−1372.

(96) Zhang, T.; Huang, C. H. Modeling the Kinetics of UV/Peracetic Acid Advanced Oxidation Process. *Environ. Sci. Technol.* **2020**, *54* (12), 7579−7590.

(97) Bulman, D. M.; Mezyk, S. P.; Remucal, C. K. The Impact of pH and Irradiation Wavelength on the Production of Reactive Oxidants during Chlorine Photolysis. *Environ. Sci. Technol.* **2019**, *53* (8), 4450−4459.

(98) Li, H.; McKay, G. Relationships between the Physicochemical Properties of Dissolved Organic Matter and Its Reaction with Sodium Borohydride. *Environ. Sci. Technol.* **2021**, *55* (15), 10843−10851.

(99) Maurer, F.; Christl, I.; Kretzschmar, R. Reduction and Reoxidation of Humic Acid: Influence on Spectroscopic Properties and Proton Binding. *Environ. Sci. Technol.* **2010**, *44* (15), 5787−5792.

(100) Li, C.; Zheng, S.; Li, T.; Chen, J.; Zhou, J.; Su, L.; Zhang, Y. N.; Crittenden, J. C.; Zhu, S.; Zhao, Y. Quantitative Structure-activity Relationship Models for Predicting Reaction Rate Constants of Organic Contaminants with Hydrated Electrons and Their Mechanistic Pathways. *Water Res.* **2019**, *151*, 468−477.

(101) Zheng, S.; Li, C.; Wei, G. QSAR Modeling for Reaction Rate Constants of e_{aq}^- With Diverse Organic Compounds in Water. *Environmental Science: Water Research & Technology* **2020**, *6* (7), 1931−1938.

(102) Liu, X.; Zhong, J.; Fang, L.; Wang, L.; Ye, M.; Shao, Y.; Li, J.; Zhang, T. Trichloroacetic Acid Reduction by an Advanced Reduction Process Based on Carboxyl Anion Radical. *Chemical Engineering Journal* **2016**, *303*, 56−63.

(103) Liu, X.; Vellanki, B. P.; Batchelor, B.; Abdel-Wahab, A. Degradation of 1,2-Dichloroethane with Advanced Reduction Processes (ARPs): Effects of Process Variables and Mechanisms. *Chemical Engineering Journal* **2014**, *237*, 300−307.

(104) Sun, C.; Chang, W.; Ma, W.; Chen, C.; Zhao, J. Photoreductive Debromination of Decabromodiphenyl Ethers in the Presence of Carboxylates Under Visible Light Irradiation. *Environ. Sci. Technol.* **2013**, *47* (5), 2370−7.

(105) Wang, L.; Liu, X. Fast Degradation of Monochloroacetic Acid by BiOI-Enhanced UV/S(IV) Process: Efficiency and Mechanism. *Catalysts* **2019**, *9* (5), 460.

(106) Yu, X.; Cabooter, D.; Dewil, R. Efficiency and Mechanism of Diclofenac Degradation by Sulfite/UV Advanced Reduction Processes (ARPs). *Sci. Total Environ.* **2019**, *688*, 65−74.

(107) Yu, X.; Cabooter, D.; Dewil, R. Effects of Process Variables and Kinetics on the Degradation of 2,4-Dichlorophenol Using Advanced Reduction Processes (ARP). *J. Hazard Mater.* **2018**, *357*, 81−88.

(108) Liu, X.; Yoon, S.; Batchelor, B.; Abdel-Wahab, A. Degradation of Vinyl Chloride (VC) by the Sulfite/UV Advanced Reduction Process (ARP): Effects of Process Variables and a Kinetic Model. *Sci. Total Environ.* **2013**, *454−455*, 578−83.

(109) Yang, Y.; Zhang, Q.; Chen, B.; Long, L.; Zhang, G. Toward Better Understanding Vacuum Ultraviolet—Iodide Induced Photolysis via Hydrogen Peroxide Formation, Iodine Species Change, and Difluoroacetic Acid Degradation. *Front. Environ. Sci. Eng.* **2022**, *16* (5), 55.

(110) Qiwen, M.; Kim, K. H.; Han, I. Correlation Analysis of Pollutant Factors Influencing the Sulfite/UV-L Advanced Reduction Process. *KSCE Journal of Civil Engineering* **2018**, *22* (2), 475−481.

(111) Yazdanbakhsh, A.; Eslami, A.; Mahdipour, F.; Ghanbari, F.; Ghasemi, S. M.; Atamaleki, A.; Maleksari, H. S.; Lin, K.-Y. A. Dye Degradation in Aqueous Solution by Dithionite/UV-C Advanced Reduction Process (ARP): Kinetic Study, Dechlorination, Degradation Pathway and Mechanism. *J. Photochem. Photobiol., A* **2021**, *407*, 112995.

(112) Wang, Z.; Liu, W.; Chen, H.; Zhang, Z.; Yang, Z.; Yang, Q. Photoreductive Degradation of CCl_4 by UV-Na_2SO_3: Influence of Various Factors, Mechanism and Application. *Environ. Technol.* **2021**, *42* (2), 217−226.

(113) Asgari, G.; Seidmohammadi, A.; Rahmani, A. R.; Samarghandi, M. R.; Faraji, H. Application of the UV/Sulfoxylate/Phenol Process in the Simultaneous Removal of Nitrate and Pentachlorophenol from the Aqueous Solution. *J. Mol. Liq.* **2020**, *314*, 113581.

(114) Cao, Y.; Qiu, W.; Li, J.; Zhao, Y.; Jiang, J.; Pang, S. Sulfite Enhanced Transformation of Iopamidol by UV Photolysis in the Presence of Oxygen: Role of Oxysulfur Radicals. *Water Res.* **2021**, *189*, 116625.

(115) Yu, X.; Gocze, Z.; Cabooter, D.; Dewil, R. Efficient Reduction of Carbamazepine Using UV-activated Sulfite: Assessment of Critical Process Parameters and Elucidation of Radicals Involved. *Chemical Engineering Journal* **2021**, *404*, 126403.

(116) Akbari, A.; Sadani, M.; Sedighizadeh, A.; Sedghi, A.; Khajeh, M.; Mahmoudi, M.; Bagheri, A.; Teimouri, F.; Behin, J. Reduction of Dinitrotoluene byHydrated Electrons Generated from UV Irradiation of Toluene in Wastewater: Towards Cleaner Production. *Journal of Cleaner Production* **2019**, *238*, 117857.

(117) Zhang, T.; Wang, J.; Yan, D.; Wang, L.; Liu, X. Efficient Reduction of Bromate by Iodide-Assisted UV/Sulfite Process. *Catalysts* **2018**, *8* (12), 652.

(118) Liu, X.; Zhang, T.; Shao, Y. Aqueous Bromate Reduction by UV Activation of Sulfite. *CLEAN - Soil, Air, Water* **2014**, *42* (10), 1370−1375.

(119) Vellanki, B. P.; Batchelor, B. Nitrate Reduction by the Ultraviolet-Sulfite Advanced Reduction Process. *Environ. Eng. Sci.* **2021**, *38*, 927.

(120) Tan, L.; Mao, R.; Su, P.; Gu, J.; Chen, H.; Jiang, F.; Zhao, X. Efficient Photochemical Denitrification by UV/Sulfite System: Mechanism and Applications. *J. Hazard Mater.* **2021**, *418*, 126448.

(121) Zhang, C.; Qu, Y.; Zhao, X.; Zhou, Q. Photoinduced Reductive Decomposition of Perflruooctanoic Acid in Water: Effect of Temperature and Ionic Strength. *CLEAN - Soil, Air, Water* **2015**, *43* (2), 223−228.

(122) Qu, Y.; Zhang, C. J.; Chen, P.; Zhou, Q.; Zhang, W. X. Effect of Initial Solution pH on Photo-induced Reductive Decomposition of Perfluorooctanoic Acid. *Chemosphere* **2014**, *107*, 218−223.

(123) Bentel, M. J.; Liu, Z.; Yu, Y.; Gao, J.; Men, Y.; Liu, J. Enhanced Degradation of Perfluorocarboxylic Acids (PFCAs) by UV/Sulfite Treatment: Reaction Mechanisms and System Efficiencies at pH 12. *Environmental Science & Technology Letters* **2020**, *7* (5), 351−357.

(124) Lyu, X. J.; Li, W. W.; Lam, P. K.; Yu, H. Q. Insights into Perfluorooctane Sulfonate Photodegradation in a Catalyst-Free Aqueous Solution. *Sci. Rep* **2015**, *5*, 9353.

(125) Guo, C.; Zhang, C.; Sun, Z.; Zhao, X.; Zhou, Q.; Hoffmann, M. R. Synergistic Impact of Humic Acid on the Photo-reductive Decomposition of Perfluorooctanoic Acid. *Chemical Engineering Journal* **2019**, *360*, 1101−1110.

(126) Anbar, M.; Hart, E. J. On the Reactivity of Hydrated Electrons Toward Inorganic Compounds. In. *Radiation Chemistry* **1968**, *81*, 79−94.

(127) Anbar, M.; Hart, E. J. Reactions of Hydrated Electron. *Solvated Electron* **1965**, *50*, 55−81.

(128) Elliot, A. J.; McCracken, D. R.; Buxton, G. V.; Wood, N. D. Estimation of Rate Constants for Near-Diffusion-Controlled Reactions in Water at High Temperatures. *J. Chem. Soc., Faraday Trans.* **1990**, *86* (9), 1539−1547.

(129) Thomas, J. K.; Gordon, S.; Hart, E. J. The Rates of Reactions of the Hydrated Electron in Aqueous Inorganic Solutions. *J. Phys. Chem.* **1964**, *68* (6), 1524−1527.

(130) Atkins, P.; Paula, J. d. *Physical Chemistry*, 7th ed.; Oxford University Press: 2003.

(131) Anbar, M. The Reactions of Hydrated Electrons with Organic Compounds. *Adv. Phys. Org. Chem.* **1969**, *7*, 115−151.

(132) Maza, W. A.; Breslin, V. M.; Owrutsky, J. C.; Pate, B. B.; Epshteyn, A. Nanosecond Transient Absorption of Hydrated Electrons and Reduction of Linear Perfluoroalkyl Acids and Sulfonates. *Environmental Science & Technology Letters* **2021**, *8* (7), 525−530.

(133) Wentworth, W. E.; Becker, R. S.; Tung, R. Thermal Electron Attachment to Some Aliphatic and Aromatic Chloro, Bromo, and Iodo Derivatives. *J. Phys. Chem.* **1967**, *71*, 1652−1665.

(134) Shoute, L. C. T.; Mittal, J. P.; Neta, P. Reduction and Defluorination of Pentafluorophenol in Aqueous Solutions. *J. Phys. Chem.* **1996**, *100*, 3016−3019.

(135) Getoff, N.; Solar, S. Radiolysis and Pulse Radiolysis of Chlorinated Phenols in Aqueous Solutions. *International Journal of Radiation Applications and Instrumentation* **1986**, *28* (5−6), 443−450.

(136) Ye, M. Radiolytic Studies of Reduction and Oxidation of Aromatic Systems. Ph.D. Thesis, Notre Dame University, 1989.

(137) Rosario-Ortiz, F. L.; Canonica, S. Probe Compounds to Assess the Photochemical Activity of Dissolved Organic Matter. *Environ. Sci. Technol.* **2016**, *50* (23), 12532−12547.

(138) Lichtscheidl, J.; Getoff, N. Radiolysis of Halogenated Aromatic Compounds in Aqueous Solutions-I Conductometric Pulse Radiolysis and Steady-State Studies of the Reaction of e_{aq}^-. *International Journal for Radiation Physics and Chemistry* **1976**, *8* (6), 661−665.

(139) Buck, R. C.; Franklin, J.; Berger, U.; Conder, J. M.; Cousins, I. T.; de Voogt, P.; Jensen, A. A.; Kannan, K.; Mabury, S. A.; van Leeuwen, S. P. Perfluoroalkyl and Polyfluoroalkyl Substances in the Environment: Terminology, Classification, and Origins. *Integr Environ. Assess Manag* **2011**, *7* (4), 513−41.

(140) Merino, N.; Qu, Y.; Deeb, R. A.; Hawley, E. L.; Hoffmann, M. R.; Mahendra, S. Degradation and Removal Methods for Perfluoroalkyl and Polyfluoroalkyl Substances in Water. *Environmental Engineering Science* **2016**, *33* (9), 615−649.

(141) Van Hoomissen, D. J.; Vyas, S. Early Events in the Reductive Dehalogenation of Linear Perfluoroalkyl Substances. *Environmental Science & Technology Letters* **2019**, *6* (6), 365−371.

(142) Vione, D.; Minella, M.; Maurino, V.; Minero, C. Indirect Photochemistry in Sunlit Surface Waters: Photoinduced Production of Reactive Transient Species. *Chemistry* **2014**, *20* (34), 10590−606.

(143) Wang, W.; Zafiriou, O. C.; Chan, I.; Zepp, R. C.; Blough, N. V. Production of Hydrated Electrons from Photoionization of Dissolved Organic Matter in Natural Waters. *Environ. Sci. Technol.* **2007**, *41* (5), 1601−1607.

(144) Dixit, F.; Barbeau, B.; Mostafavi, S. G.; Mohseni, M. Removal of Legacy PFAS and Other Fluorotelomers: Optimized Regeneration Strategies in DOM-rich Waters. *Water Res.* **2020**, *183*, 116098.

(145) Smith, B. A.; Teel, A. L.; Watts, R. J. Identification of the Reactive Oxygen Species Responsible for Carbon Tetrachloride Degradation in Modified Fenton's System. *Environ. Sci. Technol.* **2004**, *38* (20), 5465−5469.

(146) da Silva-Rackov, C. K. O.; Lawal, W. A.; Nfodzo, P. A.; Vianna, M. M. G. R.; do Nascimento, C. A. O.; Choi, H. Degradation of PFOA by Hydrogen Peroxide and Persulfate Activated by Iron-modified Diatomite. *Applied Catalysis B: Environmental* **2016**, *192*, 253−259.

(147) Panchangam, S. C.; Lin, A. Y.; Tsai, J. H.; Lin, C. F. Sonication-assisted Photocatalytic Decomposition of Perfluorooctanoic Acid. *Chemosphere* **2009**, *75* (5), 654−660.

(148) He, X.; Sun, B.; He, M.; Chi, H.; Wang, Z.; Zhang, W.; Ma, J. Highly Efficient Simultaneous Catalytic Degradation and Defluorination of Perfluorooctanoic Acid by the H_2O_2−carbon/MnO_2 System Generating O_2^- and OH Synchronously. *Applied Catalysis B: Environmental* **2020**, *277*, 119219.

(149) Javed, H.; Metz, J.; Eraslan, T. C.; Mathieu, J.; Wang, B.; Wu, G.; Tsai, A.-L.; Wong, M. S.; Alvarez, P. J. J. Discerning the Relevance of Superoxide in PFOA Degradation. *Environmental Science & Technology Letters* **2020**, *7* (9), 653−658.

(150) Neta, P.; Huie, R. E. Free-Radical Chemistry of Sulfite. *Environ. Health Perspect.* **1985**, *64*, 209−217.

(151) Sawyer, D. T.; Valentine, J. S. How Super is Superoxide? *Acc. Chem. Res.* **1981**, *14* (12), 393−400.

(152) Huang, L.; Dong, W.; Hou, H. Investigation of the Reactivity of Hydrated Electron Toward Perfluorinated Carboxylates by Laser Flash Photolysis. *Chem. Phys. Lett.* **2007**, *436* (1−3), 124−128.

(153) Szajdzinska-Pietek, E.; Gebicki, J. L. Pulse Radiolytic Investigation of Perfluorinated Surfactants in Aqueous Solutions. *Res. Chem. Intermed.* **2000**, *26*, 897−912.

(154) Benskin, J. P.; De Silva, A. O.; Martin, J. W. *Isomer Profiling of Perfluorinated Substances as a Tool for Source Tracking: A Review of Early Findings and Future Applications*; Springer: New York, 2010; Vol. *208*.

(155) Minakata, D.; Mezyk, S. P.; Jones, J. W.; Daws, B. R.; Crittenden, J. C. Development of Linear Free Energy Relationships for Aqueous Phase Radical-involved Chemical Reactions. *Environ. Sci. Technol.* **2014**, *48* (23), 13925−32.

(156) Le, T. X. H.; Haflich, H.; Shah, A. D.; Chaplin, B. P. Energy-Efficient Electrochemical Oxidation of Perfluoroalkyl Substances Using a Ti_4O_7 Reactive Electrochemical Membrane Anode. *Environmental Science & Technology Letters* **2019**, *6* (8), 504−510.

(157) Keen, O.; Bolton, J.; Litter, M.; Bircher, K.; Oppenländer, T. Standard Reporting of Electrical Energy per Order (EEO) for UV/H_2O_2 Reactors (IUPAC Technical Report). *Pure Appl. Chem.* **2018**, *90* (9), 1487−1499.

(158) Liu, C. J.; Strathmann, T. J.; Bellona, C. Rejection of Per- and Polyfluoroalkyl Substances (PFASs) in Aqueous Film-Forming Foam by High-Pressure Membranes. *Water Res.* **2021**, *188*, 116546.

(159) Naumann, R.; Lehmann, F.; Goez, M. Generating Hydrated Electrons for Chemical Syntheses by Using a Green Light-Emitting Diode (LED). *Angew. Chem., Int. Ed. Engl.* **2018**, *57* (4), 1078−1081.